NASA/CR—2008-215302 DOT/FAA/AR–07/55



# Ice Shape Scaling for Aircraft in SLD Conditions

*David N. Anderson and Jen-Ching Tsao*
*Ohio Aerospace Institute, Brook Park, Ohio*

September 2008

# NASA STI Program . . . in Profile

Since its founding, NASA has been dedicated to the advancement of aeronautics and space science. The NASA Scientific and Technical Information (STI) program plays a key part in helping NASA maintain this important role.

The NASA STI Program operates under the auspices of the Agency Chief Information Officer. It collects, organizes, provides for archiving, and disseminates NASA's STI. The NASA STI program provides access to the NASA Aeronautics and Space Database and its public interface, the NASA Technical Reports Server, thus providing one of the largest collections of aeronautical and space science STI in the world. Results are published in both non-NASA channels and by NASA in the NASA STI Report Series, which includes the following report types:

- TECHNICAL PUBLICATION. Reports of completed research or a major significant phase of research that present the results of NASA programs and include extensive data or theoretical analysis. Includes compilations of significant scientific and technical data and information deemed to be of continuing reference value. NASA counterpart of peer-reviewed formal professional papers but has less stringent limitations on manuscript length and extent of graphic presentations.

- TECHNICAL MEMORANDUM. Scientific and technical findings that are preliminary or of specialized interest, e.g., quick release reports, working papers, and bibliographies that contain minimal annotation. Does not contain extensive analysis.

- CONTRACTOR REPORT. Scientific and technical findings by NASA-sponsored contractors and grantees.

- CONFERENCE PUBLICATION. Collected papers from scientific and technical conferences, symposia, seminars, or other meetings sponsored or cosponsored by NASA.

- SPECIAL PUBLICATION. Scientific, technical, or historical information from NASA programs, projects, and missions, often concerned with subjects having substantial public interest.

- TECHNICAL TRANSLATION. English-language translations of foreign scientific and technical material pertinent to NASA's mission.

Specialized services also include creating custom thesauri, building customized databases, organizing and publishing research results.

For more information about the NASA STI program, see the following:

- Access the NASA STI program home page at *http://www.sti.nasa.gov*

- E-mail your question via the Internet to *help@sti.nasa.gov*

- Fax your question to the NASA STI Help Desk at 301–621–0134

- Telephone the NASA STI Help Desk at 301–621–0390

- Write to:
  NASA Center for AeroSpace Information (CASI)
  7115 Standard Drive
  Hanover, MD 21076–1320

NASA/CR—2008-215302 DOT/FAA/AR–07/55


# Ice Shape Scaling for Aircraft in SLD Conditions

*David N. Anderson and Jen-Ching Tsao*
*Ohio Aerospace Institute, Brook Park, Ohio*

Prepared under Cooperative Agreement NNC07BA13B

National Aeronautics and
Space Administration

Glenn Research Center
Cleveland, Ohio 44135

September 2008

## Acknowledgments

This work was jointly supported by the FAA Tech Center and the NASA Glenn Icing Branch. The authors wish to thank Jim Riley and Tom Bond of the FAA and Mark Potapczuk of NASA for their support, encouragement and valuable technical consultations and direction for several years. The late Dave Anderson initiated the SLD scaling work at NASA Glenn. Many of the early testing plans and approaches that led to results in this manual were based on Anderson's initial work. Many of the ideas for new approaches to scaling and concepts for the tests performed through the years were the result of discussions with a number of contributors, most of whom are well known in the icing community. These include Alex Feo, Mark Potapczuk, Alric Rothmayer, Mario Vargas and Bill Wright. Finally, through a number of years testing in the NASA Glenn IRT Dave Sheldon, Gary Nosky, Julius Mirecki, Bob Ide, John Oldenburg and Susan Kevdzija provided the engineering and facility support, and the IRT crew gave their ever-willing and creative technical support and patience to endure seemingly endless scaling tests on which much of the material in this manual is based. Sam Lee, Mario Vargas and Judy Van Zante gave time from their own important research to discuss, advise and assist in testing on several occasions. My grateful appreciation is extended to all these and to numerous summer interns and high-school shadowing students who helped to digitize ice shapes, reduce data and prepare figures for publications and presentations.

This report contains preliminary findings,
subject to revision as analysis proceeds.

*Level of Review*: This material has been technically reviewed by NASA technical management.

Available from

NASA Center for Aerospace Information
7115 Standard Drive
Hanover, MD 21076–1320

National Technical Information Service
5285 Port Royal Road
Springfield, VA 22161

Available electronically at http://gltrs.grc.nasa.gov

# Ice Shape Scaling for Aircraft in SLD Conditions

David N. Anderson and Jen-Ching Tsao
Ohio Aerospace Institute
Brook Park, Ohio 44142

## Nomenclature

| | |
|---|---|
| $A_c$ | Accumulation parameter, dimensionless |
| $b$ | Relative heat factor, dimensionless |
| $b_0$ | Stagnation relative heat factor, dimensionless |
| $c$ | Airfoil chord, cm |
| $c_p$ | Specific heat of air, cal/gm K |
| $c_{p,ws}$ | Specific heat of water at the surface temperature, cal/g K |
| $d$ | Cylinder diameter or twice the leading-edge radius of airfoil, cm |
| $e1$, $e2$ | Undetermined exponents, dimensionless |
| $h_c$ | Convective heat-transfer coefficient, cal/sec m$^2$ K |
| $h_G$ | Gas-phase mass-transfer coefficient, g/sec m$^2$ |
| $K$ | Inertia parameter, dimensionless |
| $K_0$ | Modified inertia parameter, dimensionless |
| $L$ | Length proportional to model chord, cm |
| $LWC$ | Cloud liquid-water content, g/m$^3$ |
| $MVD$ | Water drop median volume diameter, μm |
| $n$ | Freezing fraction, dimensionless |
| $n_0$ | Stagnation freezing fraction, dimensionless |
| $Oh$ | Ohnesorge number, dimensionless |
| $P$ | General similarity parameter, dimensionless |
| $p$ | Pressure, Pa |
| $p_w$ | Vapor pressure of water in atmosphere, Pa |
| $p_{ww}$ | Vapor pressure of water at the icing surface, Pa |
| $r$ | Recovery factor, dimensionless |
| $Re_\delta$ | Reynolds number of water drop, dimensionless |
| $s$ | Surface distance from leading edge on clean model, cm |
| $t$ | Temperature, °C |
| $t_f$ | Freezing temperature, °C |
| $t_s$ | Surface temperature, °C |
| $T$ | Absolute temperature, K |
| $V$ | Air speed, kt |
| $We_c$ | Weber number based on chord $c$ and air properties, dimensionless |
| $We_\delta$ | Weber number based on drop size and water properties, dimensionless |
| $We_L$ | Weber number based on length $L$ and water properties, dimensionless |
| $\beta$ | Collection efficiency, dimensionless |
| $\beta_0$ | Stagnation collection efficiency, dimensionless |
| $\phi$ | Drop energy transfer parameter, °C |
| $\lambda$ | Drop range, m |
| $\lambda_{Stokes}$ | Drop range if Stokes Law applies, m |
| $\Lambda_f$ | Latent heat of freezing, cal/g |
| $\Lambda_v$ | Latent heat of vaporization, cal/g |
| $\mu$ | Air viscosity, poise |
| $\theta$ | Air energy transfer parameter, °C |
| $\rho$ | Air density, kg/m$^3$ |
| $\rho_i$ | Ice density, kg/m$^3$ |
| $\rho_w$ | Liquid water density, kg/m$^3$ |
| $\sigma$ | Surface tension of water over air, N/m |
| $\tau$ | Accretion time, min |

### Subscripts

| | |
|---|---|
| $R$ | Reference |
| $S$ | Scale |
| $st$ | static |
| $tot$ | total |

## Introduction

Proposed new icing certification rules are being considered by the regulatory authorities for implementation within the next few years. These rules will supplement conditions of the FAA Title 14 of the Code of Federal Regulations (CFR) Part 25 Appendix C envelope[1] (herein referred to as Appendix C) to include testing with super-cooled large drops (SLD). When these new rules are established, test facilities will need to provide means for testing at SLD conditions or simulating them by applying scaling techniques. For example, one concern that needs to be addressed in SLD testing is to insure that large drops are supercooled. In small facilities, there may not be sufficient distance, at normal flow velocities, between the spray bars and the test section for drops to cool to the ambient temperature. For such cases, icing tests with large drops may not be possible and techniques to simulate SLD with small drops will be required.

The scaling methods discussed here can also be used to determine alternate test conditions from those desired when the latter cannot be achieved in a test facility. Scaling methods will also be needed to permit simulation of SLD cloud encounters with tests of reduced-size models. In either case, the objective is to produce a scaled ice shape ("ice shape" in this report means front main ice shape up to feather region, see fig. 4) whose non-dimensional cross-section characteristics are the

same as the reference (full size) accretion being simulated. These characteristics include leading-edge ice thickness, horn angles, horn length and horn location as shown in fig 4.

Scaling methods consist of a set of equations that are used to determine the necessary scale test conditions given the reference conditions, model size, and geometry that need to be simulated. Scaling methods developed exclusively for Appendix C conditions were described and evaluated in *Manual of Scaling Methods*[2]. These methods were developed from the work of Ruff[3] and Olsen[4] in the 1980s.

Working with Appendix C conditions only, Ruff[3] evaluated several approaches to scaling using different combinations of the parameters $K_0$, $A_c$, $n_0$, $\phi$, $\theta$, and $b$ to find an effective scaling method. He concluded that the best scaling was obtained when the parameters $K_0$, $A_c$, $n_0$, $\phi$ and $\theta$ were matched between scale and reference. Note that because of the unique relationship between $\beta_0$ and $K_0$ (eq. (6)), either of them can be used to satisfy drop trajectory. Matching the scale and reference expressions for these five parameters provides five equations to solve for five of the test conditions needed. The sixth, the temperature, pressure, velocity, *MVD* or *LWC* could be chosen arbitrarily. In Ruff's tests, velocity was generally the test condition set by the user. This approach became known as the AEDC method for the center at which the work was done. It has also been called the Ruff method. Reference 2 explained and utilized a modification of the Ruff method by including an additional similarity parameter to determine scale velocity and ignores the parameters $\phi$, $\theta$ and $b$, which are already incorporated into $n_0$. This report also uses the modified Ruff method.

The present publication supplements the Appendix C studies of reference 2 with recent data from both SLD and Appendix C tests. Only icing of unprotected surfaces will be discussed here.

Scaling issues will be reviewed briefly. Scaling results obtained by applying existing scaling methods will also be given. Within the limits of the conditions tested to date, the results show that the similarity parameters needed for Appendix C scaling also can be used for SLD scaling, and no additional parameters are required. These results were based on visual comparisons of reference and scale ice shapes. Quantification of ice shape features will be discussed later in the report. The scaling methods considered as well as these conclusions apply to the ice accreted in the leading-edge region only. For Appendix C encounters, feathers were typically not considered important, but for SLD, as well as some Appendix C conditions, feather growth can result in significant structures that cannot be ignored. Feather growth issues, including scaling approaches, need to be studied but were not fully resolved by the studies reported here. The test results presented, and thus the conclusions, were limited to NACA 0012 models with clouds with water-drop *MVD*s of 25 to 190 μm, model sizes of 27- to 183-cm chord and reference velocities of approximately 100 to 200 kt. Outside of these ranges of conditions and for other models, the physics of ice accretion may include phenomena that could change these conclusions. All tests used unswept models at 0° angle of attack.

## Similarity Parameters of Importance to Icing Scaling

Scaling depends on identifying similarity parameters – non-dimensional groupings of test conditions that are tied to icing physics. The Appendix C scaling manual[2] provides a detailed explanation of the rationale and derivations of the equations used to describe the similarity parameters involved in aircraft icing. It also includes some validation data. This section is condensed from that description, and the reader is referred to it for a more comprehensive discussion.

To scale ice shapes on unprotected surfaces when model size is scaled, only six scale test parameters, the pressure, temperature, velocity, *MVD*, *LWC* and time, need to be determined. To scale test conditions for the situation when a full-size model can be used but the facility cannot provide one of the conditions desired, many of the reference conditions can be applied unchanged. Consequently, fewer equations are needed to derive the full set of scale conditions than when size is scaled. Much of this report will address the size-scaling problem, although some discussion will consider *LWC* scaling as well.

Of the six test parameters needed to define an icing test, pressure has been the least studied. Whether or not pressure has an effect on ice shapes has been the subject of discussion for some time. Bartlett[5] concluded from past AEDC experience that pressure has "an almost insignificant effect" on ice accretion. Bartlett[6] also published ice-shape data from tests on cylinders, and reported negligible effects of pressure for the limited range of conditions considered. Oleskiw, et al[7] and De Gregorio, et al[8,9] also saw little or no effect of pressure on ice shape, within test-to-test repeatability.

While pressure is an important parameter to include in the scaling of thermal ice-protection systems, this type of scaling will not be discussed in this report. For scaling as applied to unprotected surfaces the evidence cited above indicates that pressure does not need to be

considered. More comprehensive tests to confirm the results of these pressure studies are highly desirable using large facilities with pressure capability, like the new CIRA tunnel[10,11]. In any case, for atmospheric facilities, the test-section pressure is dependent on the ambient pressure and cannot be controlled independently. In a pressure facility, the scale and reference pressures should be matched when possible. At most then, only five scale test conditions are needed, and up to five similarity parameters are required to solve for them.

Reference 2 showed that the effects of temperature and *LWC* on ice shape are interdependent; thus, one of these test conditions can be specified with the other calculated from the appropriate scaling parameter. Further evidence for this will be shown in figure 15. Consequently, only four similarity parameters are needed for complete definition of scale conditions. These four parameters will be described next.

To insure that scale and reference ice shapes are of the same size relative to the model size, it is necessary to match the potential accumulation. The first similarity parameter needed for scaling is therefore the accumulation parameter:

$$A_c = \frac{LWC\,V\,\tau}{d\,\rho_i} \tag{1}$$

If all the water drops in the path of the airfoil strike the surface and all the water impinging on the leading edge freezes at that location, $A_c$ is a measure of the thickness of ice that will accrete relative to airfoil size. Of course, we know that some water drops approaching a model will be diverted by the airflow; thus, it is necessary to consider drop inertia.

The modified inertia parameter, $K_0$, was defined by Langmuir and Blodgett[12] to describe the inertia of drops in an airstream flowing around a body:

$$K_0 = \frac{1}{8} + \frac{\lambda}{\lambda_{Stokes}}\left(K - \frac{1}{8}\right) \tag{2}$$

In equation (2), $K$ is the drop inertia parameter,

$$K = \frac{\rho_w\,MVD^2\,V}{18\,d\,\mu} \tag{3}$$

where $d$ is the radius for cylindrical models or twice the leading-edge radius for airfoils. The leading-edge radius for the NACA 0012 airfoil is 0.0158$c$ (see Abbott and von Doenhoff[13]), where $c$ is the model chord. In equation (3) *MVD* has been used for simplicity. Ideally, $K$ should be evaluated for each drop size in the cloud, resulting in an inertia distribution.

In equation (2) $\lambda/\lambda_{Stokes}$ is the drop range parameter, defined as the ratio of actual drop range to that if Stokes drag law for solid spheres applied. It is a function only of the drop Reynolds number, $Re_\delta$.

$$Re_\delta = \frac{V\,MVD\,\rho}{\mu} \tag{4}$$

Langmuir and Blodgett tabulated the values of their calculated range parameter. For convenience, the present authors curve fit those data to the following expression:

$$\frac{\lambda}{\lambda_{Stokes}} = \begin{pmatrix} 0.8388 + 0.001483\,Re_\delta \\ +0.1847\sqrt{Re_\delta} \end{pmatrix}^{-1} \tag{5}$$

Of more practical interest than $K_0$ is the collection efficiency at the stagnation line, $\beta_0$, which was shown by Langmuir and Blodgett[12] to be a function only of $K_0$,

$$\beta_0 = \frac{1.40\left(K_0 - \frac{1}{8}\right)^{0.84}}{1 + 1.40\left(K_0 - \frac{1}{8}\right)^{0.84}} \tag{6}$$

Either $\beta_0$, or its equivalent, $K_0$, is the second similarity parameter needed to address the size of accretion. By matching scale and reference values of this parameter along with $A_c$, the correct scale quantity of ice at the stagnation point can be obtained. In fact, the product $\beta_0 A_c$ determines the quantity of water that reaches the surface at the stagnation point. The fraction of water that freezes there determines the ice thickness. The freezing fraction will be discussed later. For a scale test to produce the correct non-dimensional ice thickness at the stagnation point, then, it is necessary to match both the product $\beta_0 A_c$ and freezing fraction at the stagnation point.

However, good scaling methods should ideally insure the entire ice profile, normalized to model size, of scale and reference is the same, not just that their non-dimensional thicknesses match at the stagnation point. Thus, not just $\beta_0$, but also the values of $\beta$ everywhere on the scale model should match the reference. Fortunately, for models with the same non-dimensional profile, if $\beta_0$ matches, so too will the entire $\beta$ curve over the model.

Figure 1 shows LEWICE 3.2[14,15]-generated plots of $\beta$ as a function of surface distance from stagnation for *MVD*s of 30 and 190 μm and for NACA 0012 airfoils at

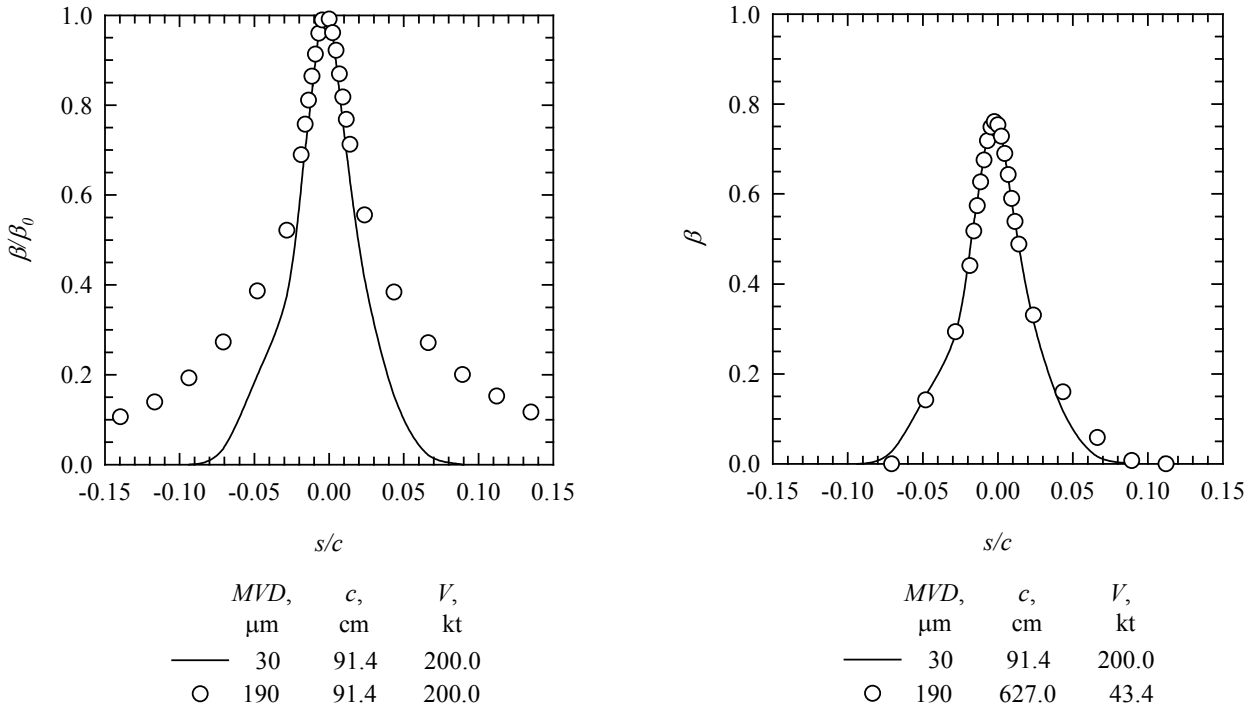


(a) Model size and velocity unchanged

(b) Stagnation collection efficiency matched.

**Figure 1.** Collection Efficiencies for Appendix C and SLD Drops Compared. NACA 0012 models at 0° AOA.

0° AOA. Figure 1 (a) compares the collection efficiency for the two *MVD*s for the same chord, 91 cm, and velocity, 200 kt. For this example, $\beta_0$ calculated from eq. (6) was 77.2% for the 30-μm case and 97.1% for the 190. To facilitate the comparison of these curves each has been plotted normalized by its respective value of $\beta_0$. Near the leading edge, the two curves are in fairly close agreement, indicating that in this portion of the airfoil the quantity of ice accreted for these two *MVD*s can be made to agree by adjusting $A_c$ so that $\beta_0 A_c$ matches, providing the freezing fraction also matches. However, for distances from the leading edge greater than 3 or 4% of chord along the surface the 190-μm case results in significantly greater water collection than the 30-μm example.

Reference 2 concluded from icing tests with Appendix C conditions that acceptable scaling results could be achieved by matching just the product $\beta_0 A_c$ when scale and reference $\beta_0$ are not matched exactly. This conclusion relaxes the scaling requirements, because there are times, usually due to facility limitations, when it is difficult or impossible to match the scale $\beta_0$ to the reference value. However, figure 1 (a) shows that this simplification may fail to scale the quantity of ice accreted away from the leading edge region when large differences between scale and reference $\beta_0$ are involved. In figure 1 (b) the conditions for the 190-μm case have been modified so that $\beta_0$ matches that of the 30-μm *MVD*. The $\beta$ curves have not been normalized. In spite of the very large difference in drop size, collection efficiencies for the two *MVD*s match virtually everywhere on the model. This result demonstrates the power, and importance, of matching $\beta_0$ as one scaling tool.

When super-cooled water drops strike an aircraft surface, they may not freeze immediately on impact. The freezing fraction is the ratio of the amount of water that freezes in a specified region on the surface to the total amount of liquid water that reaches that region. Thus, local ice thickness depends on both $\beta_0 A_c$ and freezing fraction. Because each local ice thickness around the model defines the overall shape of the ice, the freezing fraction obviously has a major influence on ice shape. The freezing fraction is influenced mainly by the ambient temperature, the *LWC* of the cloud and the aircraft velocity.

Figure 2 illustrates the way ice shapes change as freezing fraction is varied. For both Appendix C (fig. 2 (a)) and SLD (fig. 2 (b)) accretions, increasing the freezing fraction results in an increase in the thickness of ice at the stagnation point and a decrease in the included horn angle. For scaling, then, the freezing fraction has to be one of the critical similarity parameters.

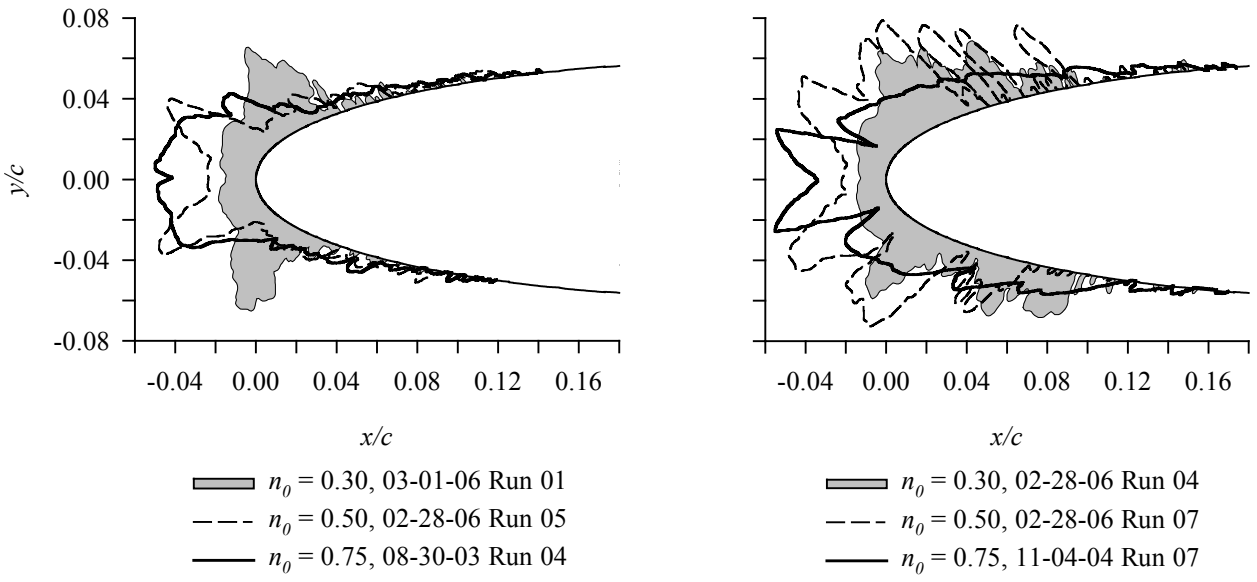


(a) Appendix C cloud.

(b) SLD cloud.

| | Date/Run | $c$, cm | $t_{st}$, °C | $t_{tot}$, °C | $V$, kt | $MVD$, μm | $LWC$, g/m$^3$ | $\tau$, min | $\beta_0$, % | $A_c$ | $\beta_0 A_c$ | $n_0$ | $We_\delta$, $10^3$ | $We_L$, $10^6$ |
|---|---|---|---|---|---|---|---|---|---|---|---|---|---|---|
| (a) | 03-01-06/01 | 91.4 | -7 | -4 | 150 | 31 | 0.63 | 22.2 | 74.4 | 2.45 | 1.82 | 0.30 | 2.85 | 2.63 |
| | 02-28-06/05 | 91.4 | -11 | -8 | 150 | 31 | 0.63 | 22.2 | 74.6 | 2.46 | 1.83 | 0.49 | 2.88 | 2.65 |
| | 08-30-03/04 | 91.4 | -16 | -13 | 150 | 28 | 0.65 | 21.7 | 71.9 | 2.46 | 1.77 | 0.76 | 2.59 | 2.63 |
| (b) | 02-28-06/04 | 91.4 | -9 | -6 | 150 | 190 | 0.73 | 14.6 | 96.7 | 1.86 | 1.80 | 0.30 | 17.3 | 2.63 |
| | 02-28-06/07 | 91.4 | -14 | -11 | 150 | 190 | 0.73 | 14.6 | 96.7 | 1.86 | 1.80 | 0.50 | 17.3 | 2.64 |
| | 11-04-04/07 | 91.4 | -24 | -21 | 149 | 160 | 0.88 | 12.1 | 95.9 | 1.85 | 1.78 | 0.75 | 14.5 | 2.62 |

**Figure 2**. Effect of Freezing Fraction on Ice Shape. $c$, 91.4 cm; $V$, 150 kt.

From Messinger's[16] surface energy balance, the stagnation freezing fraction is

$$n_0 = \frac{c_{p,ws}}{\Lambda_f}\left(\phi + \frac{\theta}{b_0}\right) \tag{7}$$

The individual terms in this expression are $\phi$, the water energy transfer parameter,

$$\varphi = t_f - t_{st} - \frac{V^2}{2c_{p,ws}} \tag{8}$$

$\theta$, the air energy transfer parameter,

$$\theta = \left(t_s - t_{st} - r\frac{V^2}{2c_p}\right) + \frac{h_G}{h_c}\left(\frac{\dfrac{p_{ww}}{T_{st}} - \dfrac{p_{tot}}{T_{tot}}\dfrac{p_w}{p_{st}}}{\dfrac{1}{.622}\dfrac{p_{tot}}{T_{tot}} - \dfrac{p_{ww}}{T_{st}}}\right)\Lambda_v \tag{9}$$

and $b$, the relative heat factor, introduced by Tribus, et. al.[17] At the stagnation line, it is:

$$b_0 = \frac{LWC\, V\, \beta_0\, c_{p,ws}}{h_c} \tag{10}$$

Equation (9) from Ruff includes compressibility effects. A simpler form without compressibility was used by Charpin and Fasso[18] and others. Ruff's expression for $\theta$ was used in the calculations for this work, but values found without compressibility are not significantly different for most icing conditions.

Bilanin[19,20] was the first to argue that drop splashing has an effect on ice accretion and that, consequently, a Weber number was a necessary similarity parameter for effective scaling methods. Bilanin believed this Weber number must be that based on drop size, $We_\delta$

$$We_\delta = \frac{V^2 MVD \rho_w}{\sigma} \tag{11}$$

to explain the effect of splashing phenomena. But reference 2 concluded that ice shapes were independent of drop size from 15 to 55 μm for constant model size and velocity provided $\beta_0 A_c$ and $n_0$ are matched ruling out $We_\delta$ as an important icing similarity parameter. SLD data to be presented below (see figs. 10 – 12) also show a lack of *MVD* effect with respect to the main ice shape (i.e., excluding the feather region). On the other hand, experiments in the IRT showed that water surface tension did indeed have a strong effect on ice shapes[20], and figure 3 shows the independent effects of surface tension and velocity at constant $\beta_0$, $A_c$, and $n_0$. This figure is a reproduction of figure 3.6.1 of reference 2 with the test conditions updated using the latest interpretation of IRT cloud *MVD*.

Figure 3 shows that horn included angles decrease either with increasing velocity or decreasing surface tension. These trends suggest that a parameter including the ratio $V^{e1}/\sigma^{e2}$, where *e1* and *e2* are unknown, must be part of a comprehensive scaling method. Consistent with Bilanin's arguments, some form of Weber number would satisfy this requirement, with *e1* = 2 and *e2* = 1. At the present time, the physics behind how this parameter affects ice shapes are not understood, although surface-water-film dynamics may be involved. Possibilities of parameters other than a Weber number that contain both a velocity and surface tension include a non-dimensional water-film height. Ultimately, more than one parameter may be required to describe fully the physics behind these results, with the velocity effects in one and surface tension in another. For now, however, a Weber number will be used.

Reference 2 discusses the variety of Weber numbers that various researchers have looked at along with some of the alternate parameters proposed to address the velocity and surface tension effects. Until we understand the physics better, reference 2 suggested using $We_L$, based on an unknown length $L$ that is proportional to the model chord. Thus,

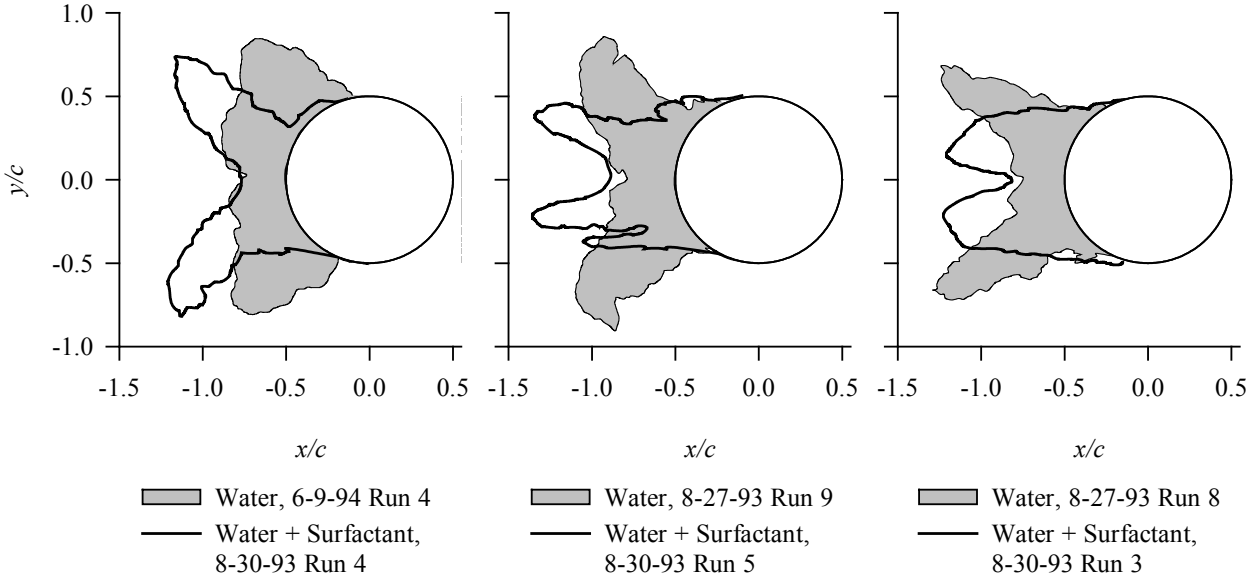


(a) $V$ = 91 kt (b) $V$ = 130 kt (c) $V$ = 182 kt

| | Date/Run | $d$, cm | $t_{st}$, °C | $t_{tot}$, °C | $V$, kt | $MVD$, μm | $LWC$, g/m$^3$ | $\tau$, min | $\sigma$, N/m | $\beta_0$, % | $A_c$ | $\beta_0 A_c$ | $n_0$ | $We_\delta$, $10^3$ | $We_L$, $10^6$ |
|---|---|---|---|---|---|---|---|---|---|---|---|---|---|---|---|
| (a) | 06-09-94/04 | 5.1 | -8 | -7 | 91 | 26 | 1.16 | 16.0 | 65 | 66.3 | 1.12 | 0.74 | 0.28 | 0.90 | 1.73 |
| | 08-30-93/04 | 5.1 | -8 | -7 | 91 | 25 | 1.17 | 16.0 | 30 | 64.0 | 1.123 | 0.72 | 0.29 | 1.80 | 3.72 |
| (b) | 08-27-93/09 | 5.1 | -12 | -10 | 130 | 29 | 1.39 | 10.2 | 65 | 73.2 | 1.22 | 0.89 | 0.30 | 2.01 | 3.51 |
| | 08-30-93/05 | 5.1 | -12 | -10 | 130 | 23 | 1.39 | 10.2 | 30 | 66.8 | 1.22 | 0.82 | 0.32 | 3.51 | 7.65 |
| (c) | 08-27-93/08 | 5.1 | -12 | -8 | 183 | 27 | 1.10 | 9.0 | 65 | 74.3 | 1.19 | 0.89 | 0.29 | 3.61 | 6.93 |
| | 08-30-93/03 | 5.1 | -12 | -8 | 182 | 22 | 1.10 | 9.2 | 30 | 68.6 | 1.22 | 0.83 | 0.30 | 6.34 | 14.90 |

**Figure 3.** Effect of Surfactant and Velocity on Appendix C Ice Shapes[2]. Vertical Cylinders Tested in the NASA Glenn IRT.

$$We_L = \frac{V^2 d \rho_w}{\sigma} \quad (12)$$

The Weber number of equation (12) has been successfully included in Appendix C scaling methods and is recommended for use in SLD scaling, as well. Examples of scaling using this parameter will be shown later in the section Recommended Scaling Methods on p 27.

To summarize, the four significant similarity parameters included in the scaling method advocated here are $\beta_0$, $A_c$ (or $\beta_0 A_c$), $n_0$ and $We_L$. As researchers obtain more understanding, other parameters may be identified. With scale model size selected, by matching scale and reference values of $We_L$ the scale velocity can be determined. By matching $\beta_0$ the scale *MVD* can be found. Reference 2 also showed that the effects of temperature and *LWC* are not independent, but interact through the freezing fraction. Therefore, with scale *LWC* chosen, by matching $n_0$ the scale temperature can be calculated. Finally, by matching $A_c$ the scale time can be established. For the scale test, then, only temperature, velocity, *MVD* and time have to be calculated from the known (reference) values of the similarity parameters.

While some of these similarity parameters are based on conditions that apply anywhere on the model, $\beta_0$ and $n_0$ are specific to the stagnation line of a clean model. Therefore, strictly speaking, scaling methods only apply at the stagnation line of a clean model. These parameters vary with chord-wise location and change as ice accretion modifies the geometry. Consequently, two assumptions are implied for scaling to be valid. The first is that with similar model geometries and similar flows around both reference and scale models, if $\beta$ and $n$ match at the stagnation point, they will tend to match everywhere on the model. This assumption has been verified for collection efficiencies in figure 1 (b). As for other airflow related issues: transition and roughness, for example, may not scale, and *Re* effects are assumed to have a minor influence on the final ice shape. Second, if the scaling is done successfully, the scale ice shape normalized by the model size will consistently agree with the reference for any accretion time starting with the clean model. Therefore, scale $\beta$ and $n$ will continue to match the respective reference values, even though those parameters are changing with time.

## Experimental Methods

The authors recorded the ice shape profiles reproduced in this report during icing tests in the NASA Glenn Icing Research Tunnel (IRT)[21]. This facility is a closed-loop, refrigerated wind tunnel with a 1.83-m-high by 2.74-m-wide test section. The temperature can be controlled[22] from -25°C to 4°C. Natural-icing clouds are simulated using arrays of air-atomizing nozzles mounted on 10 spray bars in the settling chamber upstream of the test section. The tunnel is capable of a maximum speed of nearly 350 kt in an empty test section[22]. The settling chamber is vented to the atmosphere; thus, the test-section pressure is lower than atmospheric and varies with airspeed.

All models were unswept NACA 0012 airfoils mounted vertically in the IRT with a 0° AOA. A symmetrical airfoil profile at 0° AOA was chosen to simplify scaling testing, eliminating for now the complications of lift effects. Ideally, upper- and lower-surface ice shapes would be identical, but the random nature of the ice-accretion process creates differences much like those occurring when test conditions are repeated. The use of a symmetrical airfoil provides some redundancy in ice shape recording and allows features on one surface to be captured even if they are shed from or did not form on the other. Lift effects for scale and reference cases should be the same for these tests. While future studies need to demonstrate scaling when lift is present, it is not anticipated that results with lift will change the conclusions of this report with regard to effective scaling methods.

### Uncertainty Analysis

Estimates of the uncertainty in the reported average conditions were made by considering inherent errors of instruments, temporal fluctuation and spatial variation of the instrument readings in the test section, and uncertainty in tunnel calibration of *MVD* and *LWC*. Recorded air temperature was believed to be accurate to ±0.2°C, although variations during the period of an icing spray increases the uncertainty for reported average temperatures to about ±0.5°C. The uncertainty in air velocity was estimated to be ±2 kt. For Appendix C conditions the net uncertainty in *MVD* was estimated at ±12%. For SLD conditions it may have been as much as ±20%. These uncertainties were not referenced to an absolute value of *MVD*, which was unknown. Repeatability and scatter in the *LWC* calibration data suggested the uncertainty was about ±12% for both Appendix C and SLD conditions.

These uncertainties in the test parameters led to the following uncertainty estimates in the similarity parameters: for the Appendix C tests, 4% in $\beta_0$, 12% in $A_c$, 11% in $n_0$ and 3% in $We_L$. For the SLD tests, 1% in $\beta_0$, 12% in $A_c$, 9% in $n_0$ and 3% in $We_L$. It was estimated that icing limits could be discerned within about ± 0.05 chord lengths.

Ice-Accretion Regions

Evaluations made in this report depend on comparisons between the 2-dimensional cross sections of ice accretions. It is helpful to appreciate how these profiles relate to the overall nature and appearance of the ice. For glaze ice, the complete ice structure is the result of two distinctly different growth mechanisms in different regions of the airfoil. Near the leading edge, the main growth forms from water deposited, and perhaps flowing, to cover the surface. The final accretion here is typically without significant voids. Aft of this main accretion is the feather region where feathers usually grow from a narrow base at the surface of the model and expand outward with time, forming a relatively flat structure that is trapezoidal in profile. Here, the growth occurs at a number of discrete sites, with the airfoil surface typically clean otherwise. Feather location appears to be somewhat random although scratches or irregularities in the surface of the model forward of the accretion limit are preferred sites for feather growth. While feathers appear randomly elsewhere, they will be seen at these same imperfections consistently run after run.

One explanation for the different growth regimes in glaze ice is based on how the freezing fraction varies over the model. The lowest freezing fraction occurs at the stagnation point where the water loading is greatest and increases with distance aft from there. At some location the local freezing fraction reaches unity. Forward of this location water freezes relatively slowly and is able to flow over the surface, tending to fill voids in the ice. Aft, however, water freezes rapidly on or soon after impact and is therefore unable to move from the impact site.

Feather growth and appearance have been studied by Tsao and Anderson[23,24]. They noted that feathers begin to form immediately on initiation of spray. As large feathers form, they may merge with each other to produce what may at first appear to be additional horns. Large merged feather structures often seem to act as dams for leading-edge-region water moving aft. As this water flows into the feather dams, horns are formed as part of the leading-edge accretion. Thus, feathers can often be seen merged into the aft side of horn formations. For Appendix C accretions, feathers are usually (but not always) small enough that they can be ignored. But for SLD conditions, feathers are more likely to be significant in size.

For a variety of reasons the pencil-tracing technique can give a visually misleading representation of the profile of the accretion in the feather region. Some details cannot be recorded because the pencil cannot fit into small crevices in the feather structures or spaces between feathers. Thus, in places where there are several closely spaced discrete feathers the pencil can only skip over the tops to record the feather heights, but not the feather widths. The recorded profile thus appears the same as if the ice was continuous over some chord-wise distance. In addition, feathers located above the cut line are often included in the tracing when they are too large to avoid tracing or when they appear to be more representative of the typical size and shape of feathers accreted than those at the location of the cut. On the other hand, fragile feathers are occasionally destroyed as the ice is cut, so these are lost from the record.

Because of these considerations as well as the fact that feathers are discrete not just in the chord-wise direction, but span-wise as well, the area under the ice profile in the feather region cannot be extended span wise to produce a realistic sense of the three-dimensional accretion. Nor is it valid, as it would be in the main (leading-edge) region to use the area under the feather-region ice profiles as representative of the volume of ice accreted in that region.

These points can be illustrated by comparing photographs with the corresponding ice profiles. Two examples are shown in figure 4. The 91.4-cm-chord NACA 0012 airfoil section was used in each case, and the angle of attack was 0°. Flow in each case was from left to right. A grid painted on the model can be seen in the photographs. The center horizontal line marked the model mid span, which was also the vertical center of the tunnel test section. Each grid division was 1 in (2.5 cm), and the numbers above the grid indicated the wrap distance along the surface from the stagnation line in inches. After the photographs were taken the ice was cut at the mid-span line; the tracings shown were made at that location.

Figure 4 (a) shows an Appendix C case. The velocity was 100 kt and the *MVD* 30 μm for this test. The largest feathers grew in a span-wise row (in the orientation of the photograph, this row was vertical) just aft of the main ice shape, but the sizes vary randomly along the span. Between the line where the tracing was made and 1 in below, a feather has grown large enough to merge into the aft surface of the main ice formation. Feathers growing further aft were progressively smaller in size and fewer in number. Beyond a wrap position of 3 in, only a few small feathers can be seen. The corresponding ice tracing for this test showed that up to about 3 in from the leading edge the discrete nature of feather growth was not well represented in this method of recording the ice. For tests with Appendix C conditions, like those in this example, the small feathers may not

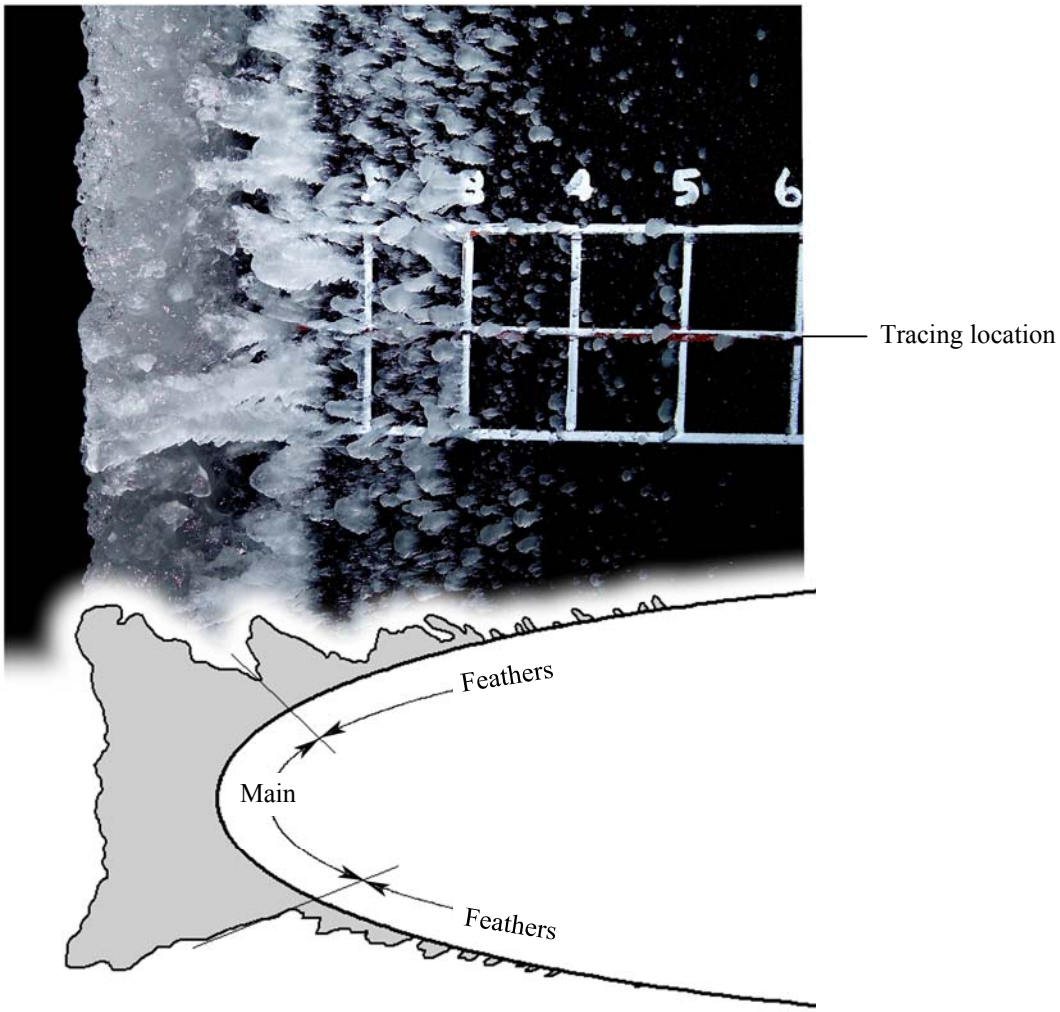


(a) Appendix C accretion. $V$, 100 kt; $MVD$, 30 μm. Test conditions shown in fig. 9 (a) for 03-01-06 run 06.

**Figure 4.** Appearance of Ice in Different Regions with Corresponding Ice Tracing. 91.4-cm-chord NACA 0012 model at 0° AOA. $n_0$, 0.50.

contribute significantly either to the aerodynamic effects of the accreted ice or to the total mass.

Figure 4 (b) gives an SLD example for a velocity of 200 kt and an *MVD* of 190 μm. For this accretion very large feathers have formed just aft of the main ice growth. These feathers formed rapidly, shielding smaller aft feathers from the spray. Consequently the aft feathers were limited to only a short time of development in the early part of the spray.

Although the tracing in figure 4 (b) might lead one to believe that there was a clear separation between the main ice and the feather region, the photograph shows that numerous small feathers were imbedded into the aft surface of the main ice. Examination of video taken during ice formation shows that feathers began to form on initiation of the spray. The most forward location of these coincided with the eventual location of horn formation. Water in the leading-edge region merged and froze into these feathers, resulting in ambiguity about the demarcation between the main ice shape and feather region. However, it is clear from the photograph that the trailing edge of the horn is randomly irregular with 3-dimensional features that cannot be captured in a 2-dimensional tracing.

Ice-Shape Repeatability

Throughout this report ice shapes from separate tests will be compared to establish effects of variables and to validate scaling methods. Therefore, it is important to understand what variations in shape are due to the random deviations inherent in ice-shape accretion and

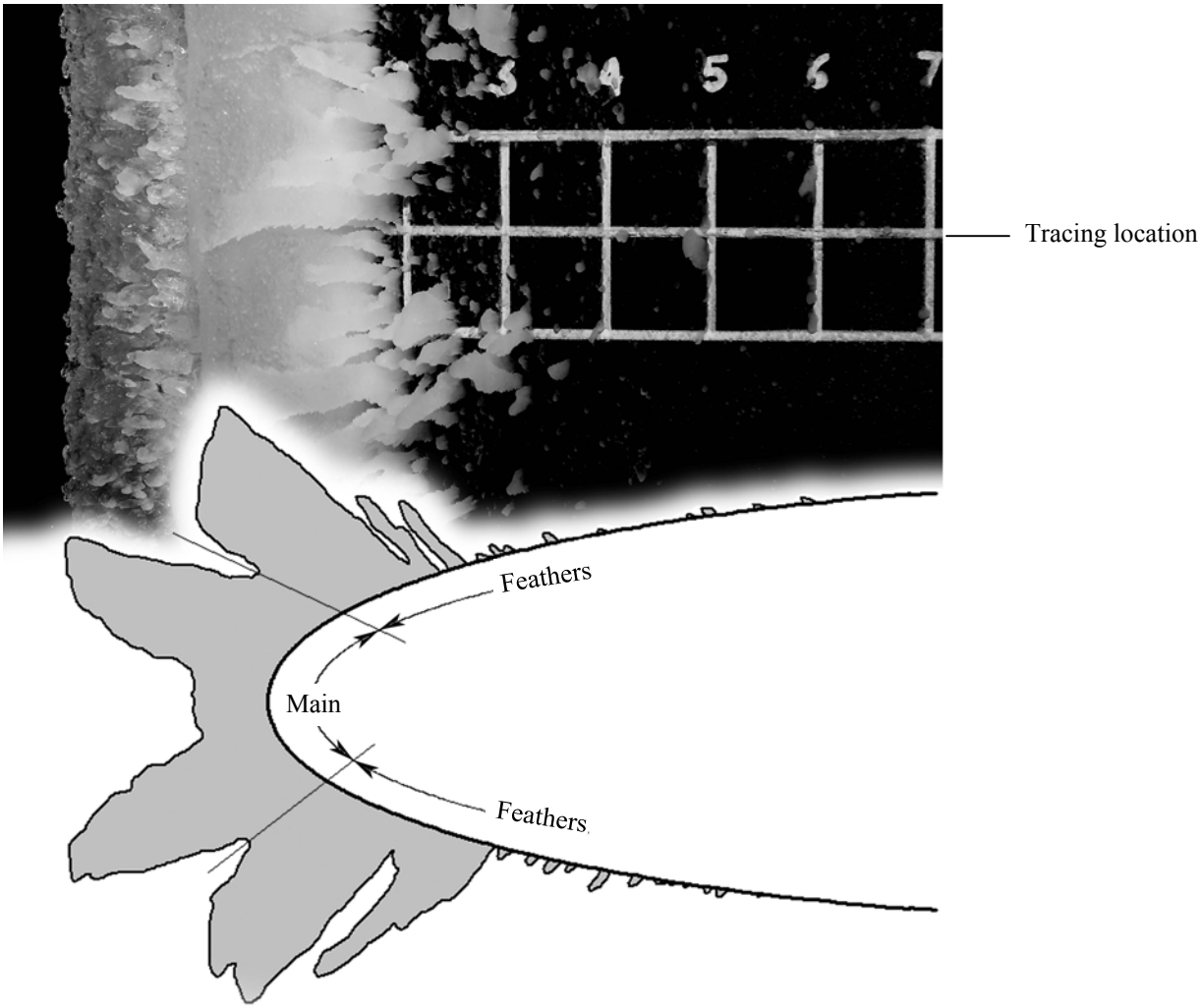


(b) SLD accretion. *V*, 200 kt; *MVD*, 190 μm. Test conditions shown in fig. 11 (d) for 02-27-06 run 06. Ice profile rotated 180° about the chord line so top surface of tracing corresponds with surface shown in photograph.

**Figure 4.** (concluded)

what can be considered significant feature distinctions that are attributable to fundamental differences in accretion physics.

Reference 2 showed that repeatability for Appendix C conditions in the IRT could be very good, even when tests were made several years apart and spanned periods when changes to the IRT spray system have been made. Figure 5 illustrates more recent repeatability results, including both Appendix C and SLD conditions. The pair of ice shape profiles in each portion of the figure was obtained during different tunnel entries with the same desired conditions or with conditions that might reasonably be expected to produce the same ice shape if tested consecutively.

The test conditions in the table included with figure 5 were not the set conditions, but rather those recorded during each test. Thus, small differences between the conditions for each pair were to be expected. For the SLD tests, the interpretation of drop-size data is continually evolving; for example, the *MVD* of a spray-bar cloud (defined by nozzle atomizing air pressure and air-water pressure difference) that was once believed to be 190 μm is now thought to be 165 – 170 μm[25]. All *MVD*s reported in this paper for IRT tests are based on the latest 2006 interpretations of IRT cloud droplet calibration data. Reference 2 showed that for constant model size and velocity changes in *MVD* over the range 15 to 55 μm have little effect on the significant features of

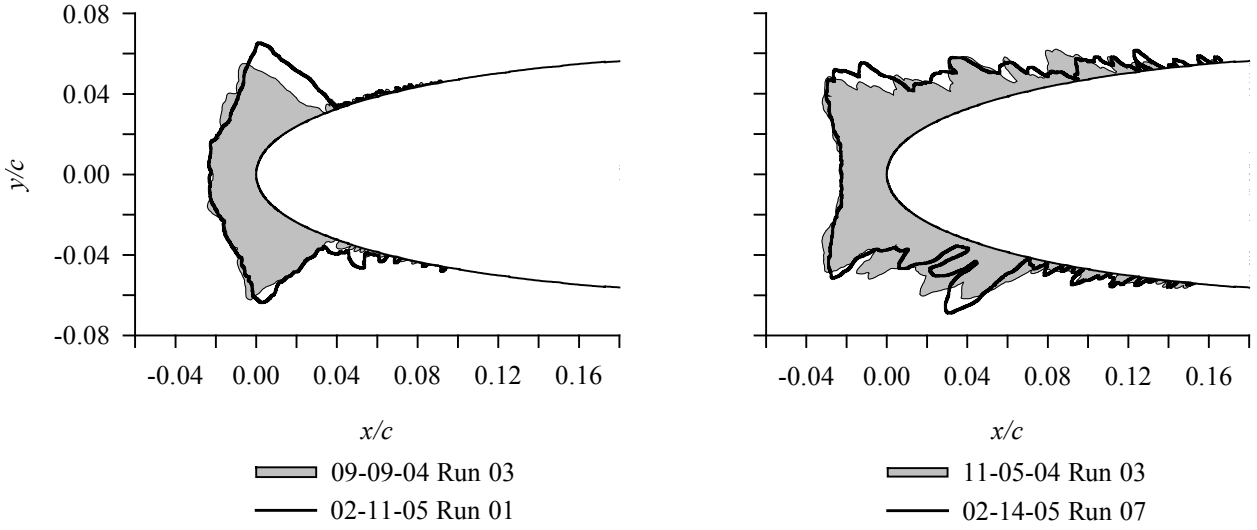


(a) Appendix C; $V$, 100 kt; $n_0$, 0.30.

(b) SLD; $V$, 100 kt; $n_0$, 0.50.

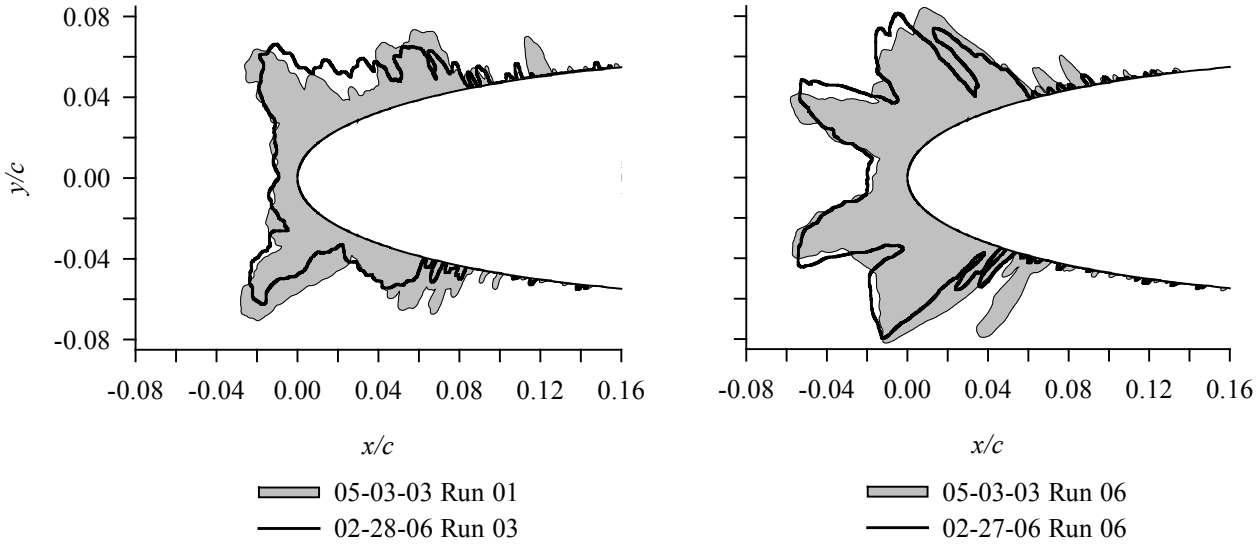


(c) SLD; $V$, 200 kt; $n_0$, 0.30.

(d) SLD; $V$, 200 kt; $n_0$, 0.50.

| | Date/Run | $c$, cm | $t_{st}$, °C | $t_{tot}$, °C | $V$, kt | $MVD$, μm | $LWC$, g/m$^3$ | $\tau$, min | $\beta_0$, % | $A_c$ | $\beta_0 A_c$ | $n_0$ | $We_\delta$, $10^3$ | $We_L$, $10^6$ |
|---|---|---|---|---|---|---|---|---|---|---|---|---|---|---|
| (a) | 09-09-04/03 | 91.4 | -6 | -4 | 100 | 26 | 0.70 | 28.0 | 64.4 | 2.28 | 1.47 | 0.35 | 1.06 | 1.17 |
| | 02-11-05/01 | 91.4 | -6 | -4 | 100 | 26 | 0.78 | 28.0 | 64.4 | 2.53 | 1.63 | 0.32 | 1.05 | 1.17 |
| (b) | 11-05-04/03 | 91.4 | -18 | -16 | 100 | 170 | 1.46 | 11.0 | 95.6 | 1.87 | 1.79 | 0.50 | 6.91 | 1.18 |
| | 02-14-05/07 | 91.4 | -18 | -16 | 99 | 165 | 1.45 | 11.2 | 95.4 | 1.88 | 1.79 | 0.50 | 6.63 | 1.16 |
| (c) | 05-03-03/01 | 91.4 | -9 | -4 | 198 | 155 | 0.48 | 16.9 | 96.3 | 1.86 | 1.79 | 0.30 | 24.8 | 4.63 |
| | 02-28-06/03 | 91.4 | -9 | -4 | 200 | 190 | 0.49 | 16.6 | 97.1 | 1.89 | 1.84 | 0.29 | 30.8 | 4.69 |
| (d) | 05-03-03/06 | 91.4 | -14 | -9 | 200 | 165 | 0.54 | 14.7 | 96.5 | 1.87 | 1.80 | 0.50 | 26.8 | 4.70 |
| | 02-27-06/06 | 91.4 | -13 | -9 | 199 | 190 | 0.49 | 16.7 | 97.1 | 1.90 | 1.84 | 0.49 | 30.7 | 4.67 |

**Figure 5**. Typical Ice-Shape Variations with Repeated Test Conditions. $c$, 91.4 cm. Mid-span tracings.

the main ice accretion, such as leading-edge thickness, and horn location, angle and size, provided $\beta_0 A_c$ and $n_0$ are matched. Further evidence of the minimal effect of *MVD* on the icing physics process for the range 30 to 190 μm will be shown in figures 10 – 12. Therefore, in figure 5 emphasis was placed on comparing accretions when the *LWC*s, rather than the *MVD*s, of the paired tests matched. All tests reported in figure 5 were made with the 91.4-cm NACA 0012 model at 0° AOA. The velocity was 100 kt for figures 5 (a) and (b), and 200 kt for (c) and (d). The small differences seen between the shapes in each pair of tests was sometimes the result of actual test conditions varying slightly from desired set values. The two Appendix C tests of figure 5 (a), for example, had identical set conditions, with a desired *LWC* of 0.80 g/m$^3$. While the same temperature, airspeed, *MVD* and time were realized for the two, the actual *LWC* for the 2005 test was about 11% higher than the 2004 due to the IRT *LWC* calibration change. This disparity resulted in a higher $\beta_0 A_c$; consequently, the area of the 2005 profile was 10% larger than for 2004. This difference was exhibited in a larger upper horn for 2005. Otherwise, the two shapes repeated well.

Most differences in shape are indicative of the somewhat random nature of ice accretion processes. In addition, methods of recording ice shapes by tracing ice accretions can lead to small variations in reported profiles. These kinds of variations are seen in the SLD examples given in figures 5 (b), (c) and (d). Horn shapes, sizes and angles can be expected to vary slightly, as shown by these figures. These differences are not considered significant. However, there is presently no well-defined sense in the icing community of how much main ice shapes can diverge before they can be considered to be significantly different. The real test of what constitutes a significant variation will depend on how changes in shape affect aerodynamic penalties.

The feather regions aft of the main ice shape can often show considerably more variety from run to run than indicated by these figures. Feather angle appears to be dependent primarily on stagnation freezing fraction[23,24], so angles should not vary when $n_0$ is matched for two tests. The size of some feathers can be affected by periodic shedding that has been observed in long icing exposures, particularly at high speeds and low freezing fractions. Fragile feathers can also be melted or bumped loose when the ice is cut to make a tracing. The preferential surface sites at which feather growth begins are known to be at small irregularities on the model surface, although feather growth is not limited to obvious imperfections. Such features may not be duplicated on models of different sizes, so locations can vary between scale and reference models. The large feathers typical of SLD tests at the higher velocities can be particularly prone to variations in size and location. Some of these differences are apparent in figure 5 (d). Considering the possible deviations, the comparisons in these figures indicate excellent repeatability of ice shape for both Appendix C and SLD conditions.

Measurements of the important features of the ice cross-sections for repeated tests were made using image-analysis software[26]. The area of the leading-edge ice, the upper horn angle and the lower horn angle were recorded. Both the mid-span tracings shown in figure 5 and the corresponding profiles traced 2.5 cm above mid span (not shown) were analyzed. The numbers are indicative of typical deviations in shape when tests are repeated, the span-wise variations in accretions and the difficulty of interpreting quantified ice features.

Results are given in Table I. The area measurements were limited to the main ice accretion, excluding feath-

Table I. Quantification of Ice Features

| Fig. | Date | Run | Tracing Location | Main Accretion Area, cm$^2$ | Upper Horn Angle, ° | Lower Horn Angle, ° |
|---|---|---|---|---|---|---|
| 5 (a) | 09-09-04 | 03 | midspan | 28.3 | 67.6 | 72.4 |
| | 09-09-04 | 03 | ms+2.5 cm | 29.5 | 64.5 | 67.5 |
| 5 (a) | 02-11-05 | 01 | midspan | 31.3 | 77.5 | 78.5 |
| | 02-11-05 | 01 | ms+2.5 cm | 26.2 | 70.5 | 78.4 |
| 5 (b) | 11-05-04 | 03 | midspan | 20.5 | 46.4 | 46.5 |
| | 11-05-04 | 03 | ms+2.5 cm | 19.0 | 45.6 | 46.3 |
| 5 (b) | 02-14-05 | 07 | midspan | 21.2 | 46.2 | 49.6 |
| | 02-14-05 | 07 | ms+2.5 cm | 19.9 | 46.3 | 49.1 |
| 5 (c) | 05-03-03 | 01 | midspan | 26.4 | 59.7 | 57.3 |
| | 05-03-03 | 01 | ms+2.5 cm | 21.3 | 56.7 | 66.2 |
| 5 (c) | 02-28-06 | 03 | midspan | 21.8 | 61.2 | 57.9 |
| | 02-28-06 | 03 | ms+2.5 cm | 19.5 | 66.2 | 55.2 |
| 5 (d) | 05-03-03 | 06 | midspan | 20.7 | 28.4 | 27.9 |
| | 05-03-03 | 06 | ms+2.5 cm | 26.1 | 22.5 | 26.9 |
| 5 (d) | 02-27-06 | 06 | midspan | 28.7 | 35.2 | 32.6 |
| | 02-27-06 | 06 | ms+2.5 cm | 27.7 | 34.9 | 33.0 |

ers for the reasons discussed in the section Ice Accretion Regions, p 8, above. However, in some cases the boundary between main ice and feather regions was not easily defined and therefore subjective. Horn angles were measured between the chord line extended upstream of the model and a straight line between the horn tip and the center of the model leading-edge radius, as shown in figure 6. Thus, horn angles were less than 90° for the examples shown. To establish the horn angle requires identification of the horn tip. For accretions for which feathers have not merged with the main ice, this can be obtained from the tracing without too much ambiguity. However, for accretions with large feather growths, some of which have merged into the horns, it is sometimes difficult to distinguish between a feather or horn tip. Thus, both area and horn angle measurements rely on subjective choices. In addition, horn angles are dependent on facility flow direction and model installation, which can be important considerations when results are compared for models of different size and for tests made at different times, as is done for tests to evaluate model-size scaling.

Table I indicates that ice-shape quantifications can sometimes vary as much as or more for tracings taken at different span-wise locations as for those recorded for repeat tests. In figure 5 (a), the mid-span cross section of 2-11-05 run 1 was about 10% larger than that of 9-9-04 run 3, due to the larger upper horn for the 2005 test. This is not an unreasonable difference in area for a repeated test, in view of uncertainties in test conditions, in particular, *LWC*. However, an even greater difference was recorded for the two tracings of 2-11-05 run 1 taken just 2.5 cm span-wise apart. The midspan cross-sectional area for the leading-edge accretion was 19% larger than that measured from a tracing taken 2.5 cm above mid-span.

Small shifts in the traced location of horns can result in important differences in the measured horn angles, as well. For run 1 on 2-11-05, the midspan horn angle was 7° larger than that recorded 2.5 cm above the midspan, while the midspan upper horn angles for the repeated tests of 9-09-04, run 3 and 2-11-05, run 1 differed by 10°. While the areas and horn angles of the shapes shown in figure 5 (b) agreed well for both repeated tests and variations along the span, the cases of figures 5 (c) and 5 (d) show much larger variations in both repeat-test and span-wise measurement comparisons.

These results show how significant variations in ice growth can take place along the span of a model. Consequently, when one attempts to quantify differences in accretions from different tests, even with the same test conditions, it is important to know that the ice shapes obtained for comparison can inherent much greater dissimilarities than are warranted. For many of the comparisons presented later, model sizes as well as test conditions for the ice accretions are not the same, and differences can be exaggerated and therefore misleading. In many cases, as suggested by Table I, repeating a test may lead to different conclusions about how well quantifications agree between two accretions.

While the quantification of ice shape features is an attractive goal that would facilitate ice-shape comparisons, the location and size of ice features tend to be somewhat random in nature and are therefore difficult to quantify in a meaningful way from cross-sectional tracings. Furthermore, for scaling comparison no method of measurement has been developed to date that provides a high level of consistency and objectivity. Therefore, ice shape agreement will be assessed by visual comparisons for the remainder of this report.

While repeatability of ice shapes has been extremely good in the IRT through the years, from time to time tests expected to result in the same ice shape can produce some large differences. Figure 7 shows two examples chosen to illustrate specific problems that need to

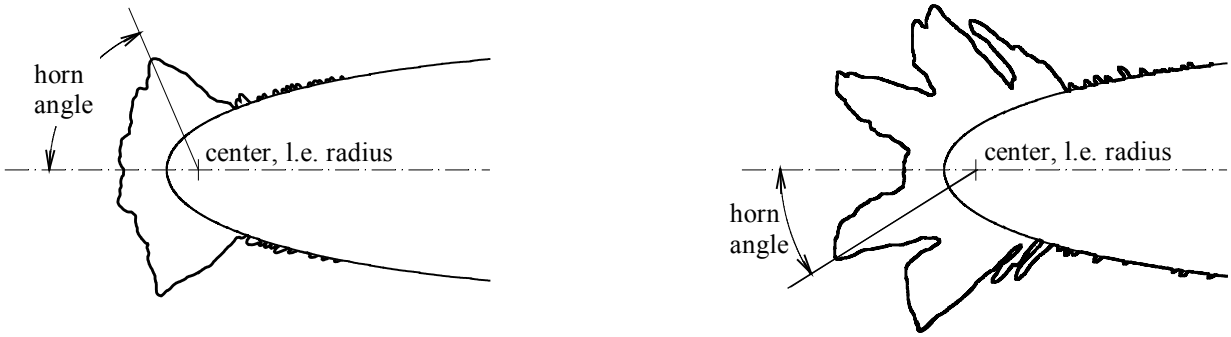


(a) Upper horn angle; ice profile of 09-09-04/03.

(b) Lower horn angle; ice profile of 02-27-06/06.

**Figure 6.** Examples of Horn Angle Definition.

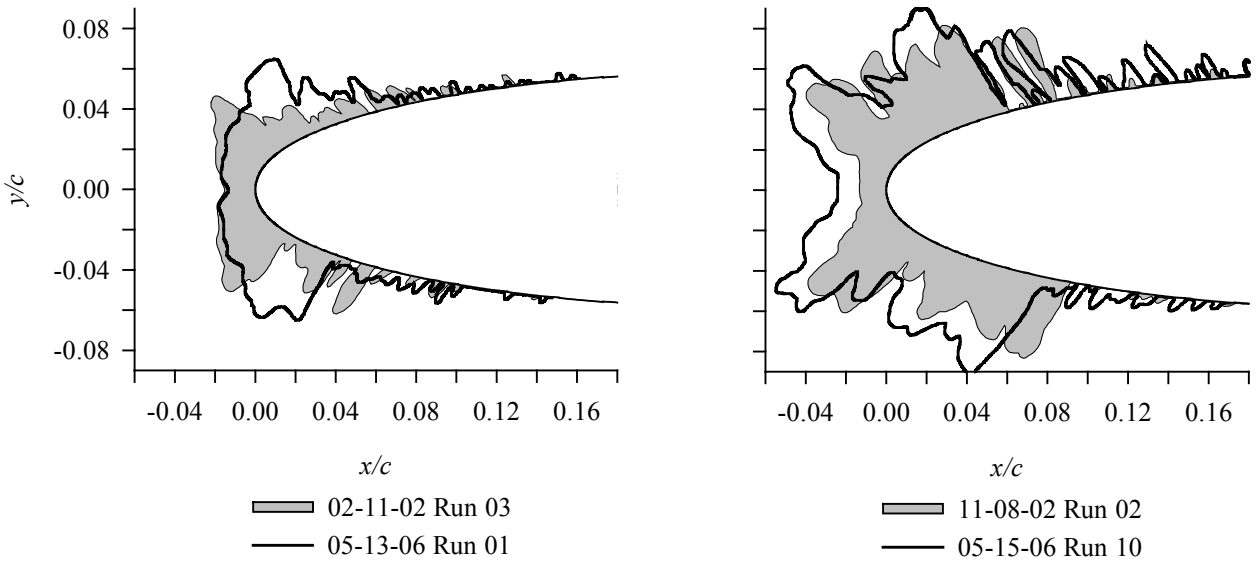


(a) Appendix C.

(b) SLD.

| | Date/Run | $c$, cm | $t_{st}$, °C | $t_{tot}$, °C | $V$, kt | $MVD$, μm | $LWC$, g/m$^3$ | $\tau$, min | $\beta_0$, % | $A_c$ | $\beta_0 A_c$ | $n_0$ | $We_\delta$, $10^3$ | $We_L$, $10^6$ |
|---|---|---|---|---|---|---|---|---|---|---|---|---|---|---|
| (a) | 02-11-02/03 | 53.3 | -9 | -6 | 148 | 35 | 1.01 | 6.8 | 84.0 | 2.02 | 1.70 | 0.31 | 3.08 | 1.50 |
| | 05-13-06/01 | 53.3 | -6 | -3 | 149 | 30 | 0.57 | 13.0 | 81.4 | 2.22 | 1.81 | 0.30 | 2.73 | 1.53 |
| (b) | 11-08-02/02 | 53.3 | -13 | -10 | 150 | 170 | 0.84 | 7.3 | 0.98 | 1.83 | 1.79 | 0.50 | 15.5 | 1.54 |
| | 05-15-06/10 | 53.3 | -12 | -9 | 150 | 190 | 0.73 | 8.4 | 0.98 | 1.84 | 1.80 | 0.50 | 17.5 | 1.56 |

**Figure 7**. Examples of non-Repeating Ice Shapes. $c$, 53.3 cm; $V$, 150 kt.

be kept in mind to avoid misinterpreting ice-shape comparisons. Figure 7 (a) is an Appendix C case, and figure 7 (b), SLD. Each of these demonstrates some of the potential difficulties involved in comparing icing results from tests performed at different times.

In figure 7 (a), the 5-13-06 test produced a larger accretion with horns swept somewhat farther back on the model than that of 2-11-02. Both of these effects can be attributed to the true *LWC* being different from the reported calibration value for one of these tests. For example, if the true *LWC* on 5-13-06 were, say, 15% higher than the calibrated value of 0.57 g/m$^3$, more ice would accrete than anticipated and, for these conditions, the true $n_0$ would be about 10% lower than shown in the table accompanying the figure. Figure 2 showed that as freezing fraction is reduced, horns move aft on the model, exactly what's seen in figure 7 (a). With an uncertainty of ±12% for the calibrated *LWC*, it is not unreasonable to expect differences of the nature seen in figure 7 (a) when comparing ice shapes, especially ones obtained with different *LWC*s.

Then how can we compare ice shapes? One should not be surprised at occasionally finding large differences. This problem can be overcome by doing extensive repeat tests and using a variety of test conditions. In addition, low freezing fraction and high $t_{tot}$ with ±0.5°C uncertainty in temperature can often make significant difference in shape when $t_{tot}$ is above –2°C.

The two profiles in figure 7 (b) also are unmatched, but for a different reason. These shapes suggest that the profiles have been translated parallel to the chord, and this is probably what has happened, in effect. When the ice tracing is made, it is necessary to melt a thin cut of ice to insert the tracing template. If this cut is not made cleanly to the surface of the model, the template cannot be inserted far enough. The result is an incorrect ice tracing showing smaller-than-actual ice thickness at the leading edge and other features translated chord-wise.

The validity of methods to produce properly scaled ice shapes depends on evaluating comparisons between two ice shapes obtained with unmatched test conditions and frequently with unlike model sizes tested at different

times. The examples of figure 7 serve to warn that ice accretions may not always behave as expected.

Effect of Model Size and Test Conditions

Reference 2 looked at parameter effects in Appendix C conditions. In this report, the effect of parameters will also be shown for SLD in order to determine if the effects are different in the two regimes.

Model size

If model size had no independent effect on non-dimensional ice shape, there would be no need to perform scaling calculations when a reduced-size model is to be tested. Thus, it is interesting to see how size affects ice shape. Examples of shapes recorded on models of 26.7-, 91.4- and 182.9-cm chord are shown in figure 8, where the ice-shape coordinates are normalized by the chord of the model. The freezing fraction was approximately 0.5 for all tests. The velocity was 100 kt for figure 8 (a) and (b) and 200 kt for 8 (c) and (d). Accretions for both Appendix C (fig. 8 (a) and (c)) and SLD (fig. 8 (b) and (d)) conditions are shown.

With constant freezing fraction, the angle included between the horns decreased as model size increased. Although the horn angle has also been shown to decrease with increasing freezing fraction (fig. 2), the leading edge thickness also increased with $n_0$, but not with chord. Therefore, it is not possible to perform size scaling simply by adjusting freezing fraction.

Velocity

The effect of velocity on ice shape was seen in figure 3 for cylinders over a range of approximately 90 to 180 kt. As velocity increased, the included horn angle decreased much the same way it did in figure 2 when freezing fraction increased, but without affecting the leading-edge thickness. Figure 9 illustrates that same effect for the 91-cm-chord NACA 0012 model for velocities of 100, 150 and 250 kt. For all tests, the simi-

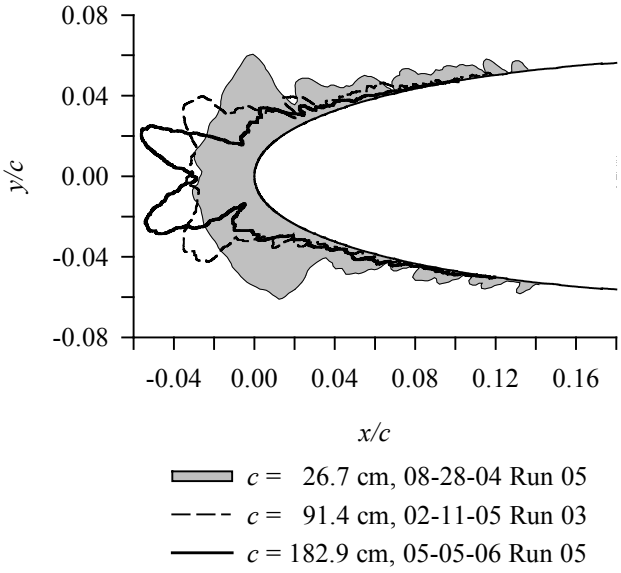


(a) Appendix C cloud; $V$, 100 kt.

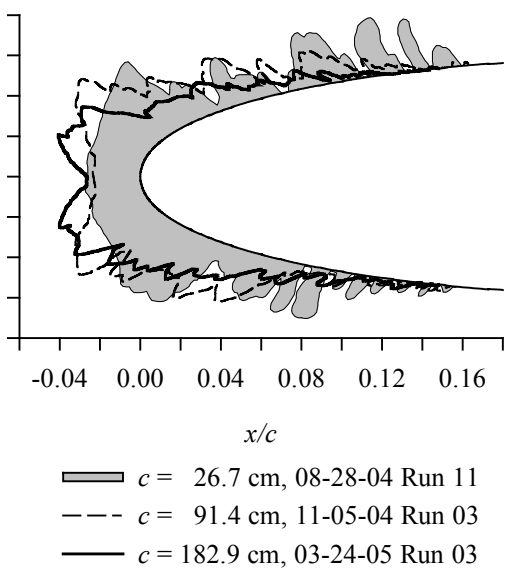


(b) SLD cloud; $V$, 100 kt.

| | Date/Run | $c$, cm | $t_{st}$, °C | $t_{tot}$, °C | $V$, kt | $MVD$, μm | $LWC$, g/m$^3$ | $\tau$, min | $\beta_0$, % | $A_c$ | $\beta_0 A_c$ | $n_0$ | $We_\delta$, $10^3$ | $We_L$, $10^6$ |
|---|---|---|---|---|---|---|---|---|---|---|---|---|---|---|
| (a) | 08-28-04/05 | 26.7 | -7 | -7 | 100 | 26 | 0.71 | 6.8 | 84.9 | 1.90 | 1.60 | 0.55 | 1.05 | 0.34 |
| | 02-11-05/03 | 91.4 | -9 | -9 | 100 | 26 | 0.78 | 28.0 | 64.5 | 2.54 | 1.64 | 0.54 | 1.06 | 1.18 |
| | 05-05-06/05 | 182.9 | -17 | -17 | 100 | 30 | 1.74 | 32.5 | 54.9 | 3.29 | 1.80 | 0.50 | 1.21 | 2.33 |
| (b) | 08-28-04/11 | 26.7 | -11 | -11 | 99 | 135 | 1.19 | 3.6 | 97.8 | 1.70 | 1.66 | 0.53 | 5.42 | 0.34 |
| | 11-05-04/03 | 91.4 | -18 | -18 | 100 | 170 | 1.46 | 11.0 | 95.6 | 1.87 | 1.79 | 0.50 | 6.91 | 1.18 |
| | 03-24-05/03 | 182.9 | -21 | -21 | 100 | 170 | 1.45 | 22.9 | 92.3 | 1.93 | 1.78 | 0.50 | 6.91 | 2.35 |

**Figure 8**. Effect of Model Size on Ice Shape. NACA 0012 Airfoils at 0°AOA; $n_0 = 0.50$.

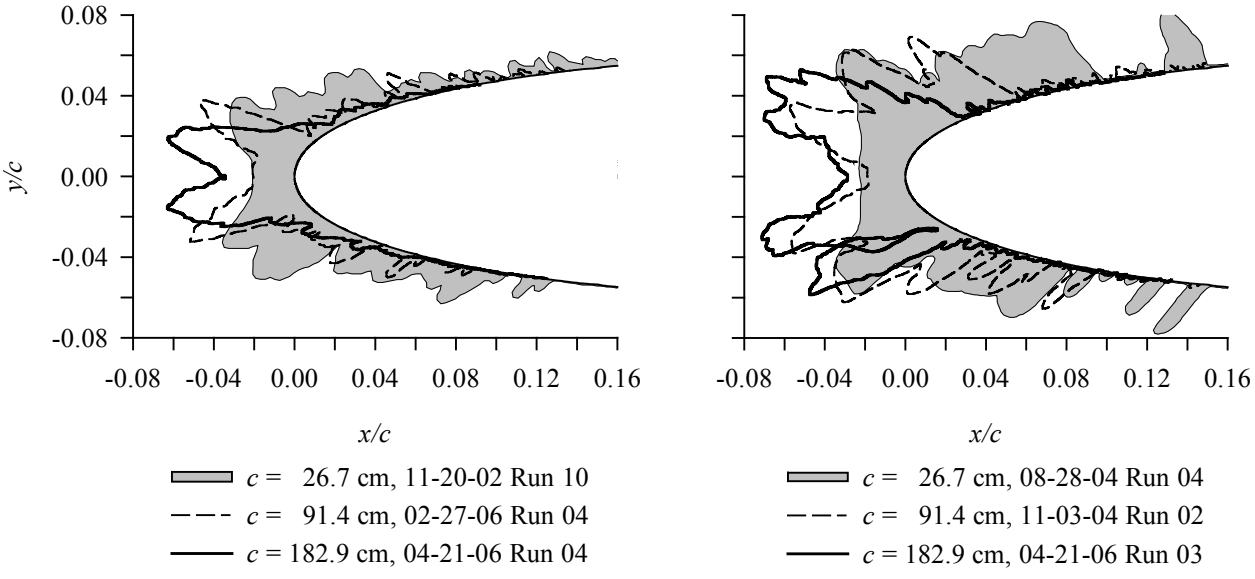


(c) Appendix C cloud; $V$, 200 kt..

(d) SLD cloud; $V$, 200 kt..

| | Date/Run | $c$, cm | $t_{st}$, °C | $t_{tot}$, °C | $V$, kt | $MVD$, μm | $LWC$, g/m$^3$ | $\tau$, min | $\beta_0$, % | $A_c$ | $\beta_0 A_c$ | $n_0$ | $We_\delta$, $10^3$ | $We_L$, $10^6$ |
|---|---|---|---|---|---|---|---|---|---|---|---|---|---|---|
| (c) | 11-20-02/10 | 26.7 | -12 | -7 | 200 | 32 | 0.80 | 3.0 | 90.8 | 1.92 | 1.75 | 0.51 | 5.18 | 1.37 |
| | 02-27-06/04 | 91.4 | -12 | -7 | 200 | 31 | 0.51 | 19.7 | 77.2 | 2.35 | 1.82 | 0.49 | 5.07 | 4.68 |
| | 04-21-06/04 | 182.9 | -20 | -15 | 199 | 30 | 1.10 | 22.0 | 64.0 | 2.82 | 1.80 | 0.50 | 4.85 | 9.35 |
| (d) | 08-28-04/04 | 26.7 | -10 | -5 | 200 | 135 | 0.51 | 4.1 | 98.4 | 1.67 | 1.64 | 0.54 | 22.0 | 1.37 |
| | 11-03-04/02 | 91.4 | -13 | -8 | 200 | 125 | 0.49 | 16.5 | 95.2 | 1.88 | 1.79 | 0.50 | 20.3 | 4.70 |
| | 04-21-06/03 | 182.9 | -14 | -9 | 200 | 140 | 0.40 | 41.8 | 92.7 | 1.95 | 1.80 | 0.50 | 22.8 | 9.40 |

**Figure 8**. (concluded).

larity parameter $\beta_0 A_c$ was approximately 1.8 and $n_0$ was 0.5.

Figure 9 (a) shows results for Appendix C conditions, while 9 (b) is for SLD. The velocity effect is the same for both regimes, and the main SLD ice shapes appear to be very similar to the Appendix C, as well. Shape profiles in the two regimes will be compared directly in the next section, where the effect of drop size will be discussed. Note that the change in horn angle appears to be greater when the velocity is increased from 100 to 150 kt than in the interval from 150 to 250 kt. In fact, the variation between profiles at 150 and 250 kt was not significantly greater than can sometimes occur when tests are repeated at the same conditions. For some test series with this model where $\beta_0 A_c$ and $n_0$ were maintained but with $V$ increasing, ice shapes changed from 100 to 150 kt, and then remained the same for 150, 200 and 250 kt.

Additional tests need to be performed with a view to understanding the physics behind these velocity effects, to determine if there are limiting velocities above which no further change in shape occurs, and, if so, to establish relationships between those limiting velocities and the model sizes and test conditions for which they occur. If there is a limiting velocity above which ice accretions do not change shape, future studies may show that for some situations, scale velocities can simply match the reference. They would not need to be as high as those required matching $We_L$ between scale and reference conditions, and, consequently, higher reference velocities could be scaled. However, until more is understood, the safest scaling approach is to match the $We_L$ defined in equation (12).

Drop Size

This section reviews and evaluates concerns with respect to ice-accretion physics for SLD that may be dif-

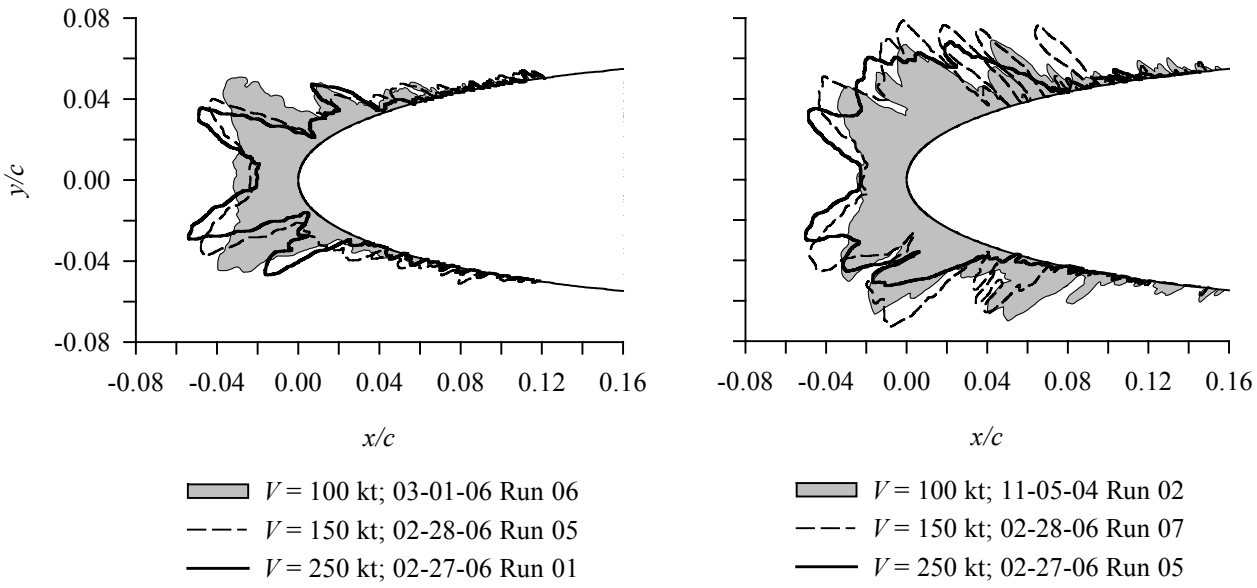


(a) Appendix C. (b) SLD.

| | Date/Run | $c$, cm | $t_{st}$, °C | $t_{tot}$, °C | $V$, kt | $MVD$, μm | $LWC$, g/m$^3$ | $\tau$, min | $\beta_0$, % | $A_c$ | $\beta_0 A_c$ | $n_0$ | $We_\delta$, $10^3$ | $We_L$, $10^6$ |
|---|---|---|---|---|---|---|---|---|---|---|---|---|---|---|
| (a) | 03-01-06/06 | 91.4 | -10 | -8 | 100 | 31 | 0.84 | 26.7 | 70.2 | 2.61 | 1.83 | 0.49 | 1.3 | 1.17 |
| | 02-28-06/05 | 91.4 | -11 | -8 | 150 | 31 | 0.63 | 22.2 | 74.6 | 2.46 | 1.83 | 0.49 | 2.9 | 2.65 |
| | 02-27-06/01 | 91.4 | -14 | -6 | 250 | 31 | 0.43 | 18.4 | 79.3 | 2.30 | 1.82 | 0.50 | 8.0 | 7.36 |
| (b) | 11-05-04/02 | 91.4 | -17 | -15 | 100 | 175 | 1.29 | 12.4 | 95.7 | 1.86 | 1.78 | 0.50 | 7.1 | 1.18 |
| | 02-28-06/07 | 91.4 | -14 | -11 | 150 | 190 | 0.73 | 14.6 | 96.7 | 1.86 | 1.80 | 0.50 | 17.3 | 2.64 |
| | 02-27-06/05 | 91.4 | -15 | -8 | 250 | 190 | 0.41 | 15.4 | 97.3 | 1.86 | 1.81 | 0.50 | 48.5 | 7.37 |

**Figure 9**. Effect of Velocity on Ice Shape. $c$, 91.4 cm; $n_0$, 0.5.

ferent from Appendix C icing conditions. These physical processes include the distortion and breakup of large drops before impact and splashing of drops on impact. If significant, different physics could necessitate including new similarity parameters in the scaling methods developed for Appendix C clouds. Such changes, however, do not appear to be necessary for the *MVD*s tested to date. Evidence, in the form of ice shapes, will be presented to evaluate the significance of these large-drop effects on scaling methods. Again, the ice shape in this report means main ice shape up to feather region.

Luxford, Hammond and Ivey[27] investigated drop distortion and breakup for conditions of aircraft exposure to SLD clouds. Considerations of not just the value of $We_\delta$ but of the transient exposure of the drop to changing inertia forces in the vicinity of the model led the authors to conclude that distortion and breakup events would not be possible to scale. When drops penetrate rapidly to the surface, such as when a small model is involved, there is insufficient time for distortion or breakup. For large models, however, there is time for these events to occur. The implication for SLD scaling is that it may be risky to apply scaling methods to reference models larger than those on which the methods have been tested. The largest model tested in the present studies had a chord of 183 cm. It is not known at this time if this model is large enough to experience droplet distortion and breakup phenomena.

Wright and Potapczuk[28] made an extensive evaluation of a number of physical processes not presently included in LEWICE to determine which might lead to significant changes in ice accretion predictions. Their conclusion was that the addition of a drop distortion and breakup model would not have a significant effect on calculated ice shapes, while the addition of a splashing model with mass loss might have some effect near the icing limit.

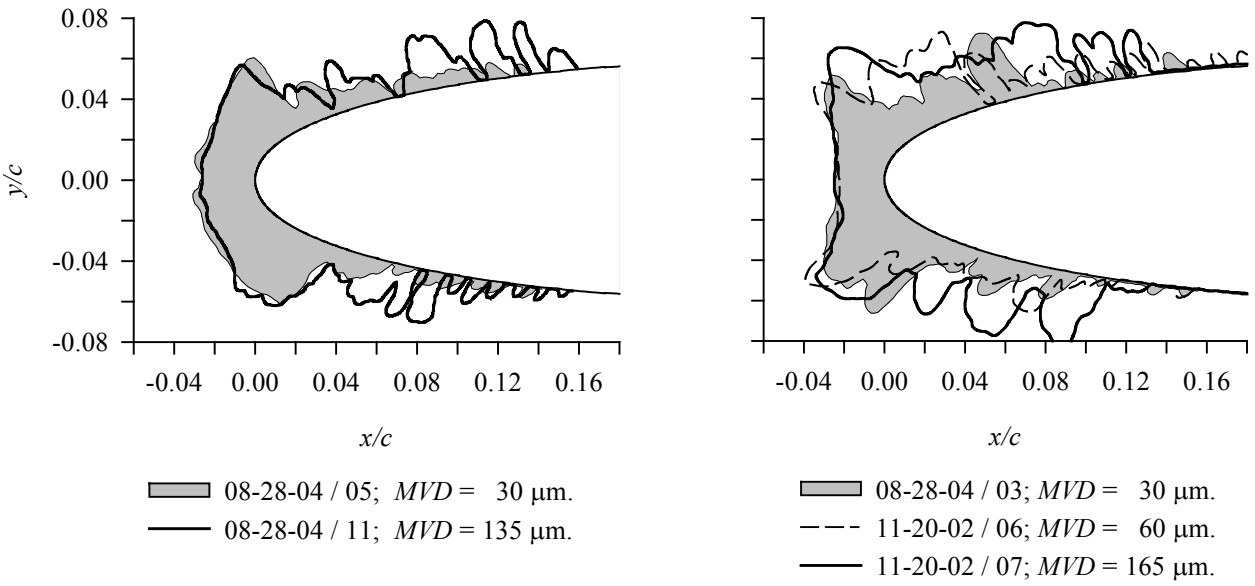


(a) $V$, 100 kt.

(b) $V$, 200 kt.

| | Date/Run | $c$, cm | $t_{st}$, °C | $t_{tot}$, °C | $V$, kt | $MVD$, μm | $LWC$, g/m$^3$ | $\tau$, min | $\beta_0$, % | $A_c$ | $\beta_0 A_c$ | $n_0$ | $We_\delta$, $10^3$ | $We_L$, $10^6$ |
|---|---|---|---|---|---|---|---|---|---|---|---|---|---|---|
| (a) | 08-28-04/05 | 26.7 | -7 | -5 | 100 | 30 | 0.70 | 6.8 | 86.4 | 1.90 | 1.64 | 0.54 | 1.2 | 0.34 |
| | 08-28-04/11 | 26.7 | -11 | -10 | 99 | 135 | 1.19 | 3.6 | 97.8 | 1.70 | 1.66 | 0.53 | 5.4 | 0.34 |
| (b) | 08-28-04/03 | 26.7 | -10 | -4 | 200 | 30 | 0.50 | 4.6 | 90.1 | 1.84 | 1.66 | 0.53 | 4.9 | 1.37 |
| | 11-20-02/06 | 26.7 | -10 | -5 | 199 | 60 | 0.53 | 4.4 | 95.7 | 1.85 | 1.78 | 0.51 | 9.7 | 1.36 |
| | 11-20-02/07 | 26.7 | -10 | -5 | 200 | 165 | 0.55 | 4.2 | 98.7 | 1.85 | 1.82 | 0.50 | 26.9 | 1.38 |

**Figure 10**. Effect of Drop Size on Ice Shape for a Chord of 26.7 cm. $n_0$, 0.50.

Drop impact studies have identified parameters with which splashing can be correlated[29,30]. Reference 30 introduced the $K$ factor (not to be confused with Langmuir and Blodgett's inertia parameter), $K = Oh\ Re_\delta^{1.25}$, where $Oh = We_\delta^{1/2}/Re_\delta$ is the Ohnesorge number. In these relationships, both $We_\delta$ and $Re_\delta$ are based on the drop $MVD$ and water properties. The $K$ factor increases with velocity and $MVD$, and splashing only occurs when $K$ is greater than a threshold value. Typically, $K$ will be greater for SLD drop sizes than for those within Appendix C. Whether this $K$ factor or its splashing threshold applies in icing conditions is not known, but it is widely believed that splashing in SLD conditions could have a much greater effect on ice accretion than it does for Appendix C clouds. If that is so, scaling for drops above some yet-to-be-determined $MVD$ size could well require new scaling approaches.

Potapczuk[31] weighed the ice accreted over a portion of the span of NACA 0012 models and compared the results with LEWICE predictions of the quantity of ice. For large drops, LEWICE predicted greater weight of ice than was measured. Furthermore, the weight difference increased with $MVD$ up to 200 μm. These results suggested splashing and mass loss in the experiments, since LEWICE at that time had no mechanism for mass loss. However, some doubt about the validity of LEWICE predictions in the SLD regime prompted further experiments, also reported in reference 31, in which a series of tests were made to compare SLD and Appendix C ice weights when similarity parameters governing accumulation were held constant. The results of these tests were inconclusive with regard to mass loss for SLD conditions. Unfortunately, the latter series of experiments required that the SLD tests be performed at low speeds to match collection efficiencies with those for Appendix C drops; at low velocities, mass loss might be expected to be minimal.

Papadakis, et al[32] published images of splashing at the leading edge of an airfoil exposed to clouds with $MVDs$

of 94- and 270-μm. The authors also measured collection efficiencies for six airfoil shapes with reported *MVD*s of 79, 137 and 168 μm. The experimental $\beta$s were compared with values predicted by LEWICE and found to be lower aft of the leading-edge region. The disparity was attributed to splashing, since the LEWICE model used did not account for splashing and re-entrainment of ejected drops. Although differences between experiment and LEWICE were significant aft of the leading-edge region, the $\beta_0$ values were in agreement within experimental uncertainty for even the largest drops tested.

Other researchers have performed splashing studies as well. These include Rutkowski, et al[33], Tan and Papadakis[34] and Gent, et al[35,36]. Most such studies were made at above-freezing temperatures, and none have actually shown the effect of large-drop splashing on ice accretion shapes.

To determine possible changes in ice shape as the drop size increased from Appendix C to SLD, a parametric study of the effect of *MVD* on the ice shape was performed at NASA Glenn using NACA 0012 airfoils at 0°AOA. *MVD* ranged from 30 through 190 μm, for model chords from 27 to 183 cm, for freezing fractions of 0.30 and 0.50, and for velocities of 100 and 200 kt. Results are shown in figures 10, 11 and 12.

Figure 10 presents ice shapes recorded for a 27-cm-chord NACA 0012 at a stagnation freezing fraction of 0.50. 10 (a) compares a 30-μm-*MVD* shape with one obtained at an *MVD* of 135 μm for a velocity of 100 kt. The leading-edge shape for these two *MVD*s was nearly identical in shape and size, but the larger drop cloud produced much larger feathers.

The ice shapes in figure 10 (b) were obtained with the same model and stagnation freezing fraction as (a), but with a velocity of 200 kt. Results of a 30-μm-*MVD* test are compared with those from tests with *MVD*s of 60 and 165 μm. Again, there was not a significant difference between the leading-edge shape obtained in an Appendix C cloud and those for SLD clouds, although

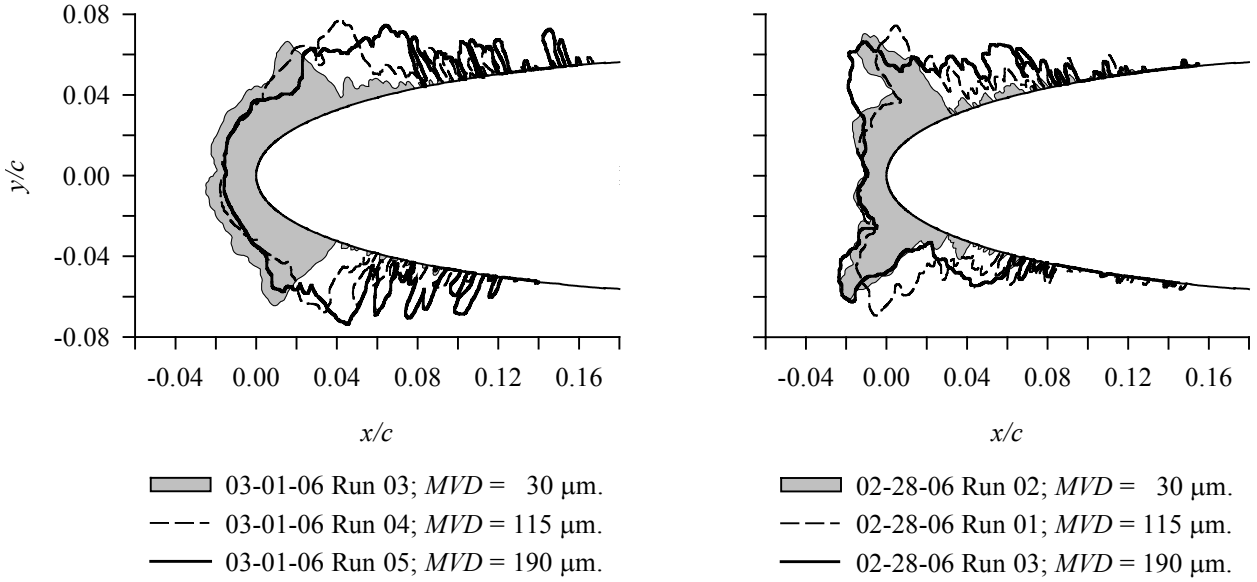


(a) *V*, 100 kt; $n_0$, 0.30.

(b) *V*, 200 kt; $n_0$, 0.30.

| | Date/Run | *c*, cm | $t_{st}$, °C | $t_{tot}$, °C | *V*, kt | *MVD*, μm | *LWC*, g/m$^3$ | $\tau$, min | $\beta_0$, % | $A_c$ | $\beta_0 A_c$ | $n_0$ | $We_\delta$, $10^3$ | $We_L$, $10^6$ |
|---|---|---|---|---|---|---|---|---|---|---|---|---|---|---|
| (a) | 03-01-06/03 | 91.4 | -6 | -5 | 100 | 30 | 0.84 | 26.7 | 70.2 | 2.61 | 1.83 | 0.30 | 1.3 | 1.17 |
| | 03-01-06/04 | 91.4 | -8 | -6 | 100 | 115 | 0.90 | 18.5 | 92.9 | 1.94 | 1.80 | 0.30 | 4.7 | 1.17 |
| | 03-01-06/05 | 91.4 | -10 | -8 | 100 | 190 | 1.27 | 12.7 | 96.1 | 1.87 | 1.80 | 0.30 | 7.7 | 1.17 |
| (b) | 02-28-06/02 | 91.4 | -8 | -3 | 200 | 30 | 0.51 | 19.7 | 77.2 | 2.36 | 1.82 | 0.29 | 5.1 | 4.69 |
| | 02-28-06/01 | 91.4 | -8 | -2 | 200 | 115 | 0.37 | 22.7 | 94.7 | 1.95 | 1.85 | 0.29 | 18.6 | 4.69 |
| | 02-28-06/03 | 91.4 | -9 | -4 | 200 | 190 | 0.49 | 16.6 | 97.1 | 1.89 | 1.84 | 0.29 | 30.8 | 4.69 |

**Figure 11**. Effect of Drop Size on Ice Shape for a Chord of 91.4 cm.

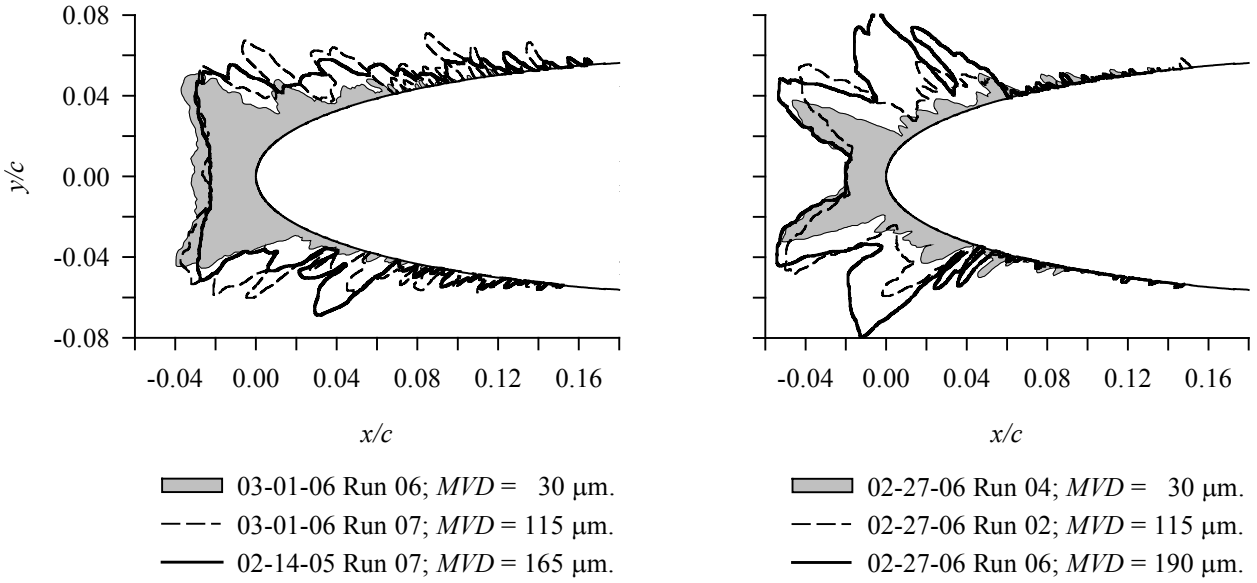


(c) $V$, 100 kt; $n_0$, 0.50.

(d) $V$, 200 kt; $n_0$, 0.49.

| | Date/Run | $c$, cm | $t_{st}$, °C | $t_{tot}$, °C | $V$, kt | $MVD$, μm | $LWC$, g/m$^3$ | $\tau$, min | $\beta_0$, % | $A_c$ | $\beta_0 A_c$ | $n_0$ | $We_\delta$, $10^3$ | $We_L$, $10^6$ |
|---|---|---|---|---|---|---|---|---|---|---|---|---|---|---|
| (c) | 03-01-06/06 | 91.4 | -10 | -8 | 100 | 30 | 0.84 | 26.7 | 70.2 | 2.61 | 1.83 | 0.49 | 1.3 | 1.17 |
| | 03-01-06/07 | 91.4 | -13 | -11 | 100 | 115 | 0.90 | 18.5 | 92.9 | 1.93 | 1.80 | 0.50 | 4.6 | 1.17 |
| | 02-14-05/07 | 91.4 | -18 | -16 | 99 | 165 | 1.45 | 11.2 | 95.4 | 1.88 | 1.79 | 0.50 | 6.6 | 1.16 |
| (d) | 02-27-06/04 | 91.4 | -12 | -7 | 200 | 30 | 0.51 | 19.7 | 77.2 | 2.35 | 1.82 | 0.49 | 5.1 | 4.68 |
| | 02-27-06/02 | 91.4 | -11 | -6 | 200 | 115 | 0.37 | 22.8 | 94.7 | 1.96 | 1.86 | 0.49 | 18.7 | 4.69 |
| | 02-27-06/06 | 91.4 | -13 | -8 | 199 | 190 | 0.49 | 16.7 | 97.1 | 1.90 | 1.84 | 0.49 | 30.7 | 4.67 |

**Figure 11**. (concluded).

the 165-μm horns were somewhat larger than those for the smaller *MVD*s. This difference can be explained by higher collection efficiencies aft of the leading edge for the larger *MVD*. Thus, again, fundamental differences in ice-accretion physics were not apparent between Appendix C and SLD. Increasing the cloud drop size again increased the feather sizes.

The effect of *MVD* on ice shape when the model chord was increased to 91 cm is shown in figure 11. Parts (a) and (b) present results for a stagnation freezing fraction of 0.30, while (c) and (d) are for $n_0$ = 0.50. But why choose $n_0$ of 0.3 and 0.5? First of all, 0.3 is the minimum $n_0$ value for practical testing. Secondly, 0.5 is a practical glaze condition with significant features that depend on scaling methods. As $n_0 \rightarrow 1$, ice shapes became less and less sensitive to scaling parameters as long as $n_0$ was matched. (a) and (c) were obtained at a velocity of 100 kt and (b) and (d) at 200 kt. For both figures 11 (a) and (b) ice tracings for *MVD*s of 30, 115 and 190 μm are shown.

At these conditions, the effect of *MVD* on ice shape was small. At a velocity of 100 kt and a stagnation freezing fraction of 0.30 (11 (a)), the horns for the SLD cases were further aft than for the 30-μm test with a slightly reduced ice thickness around the leading edge. Differences like these have also been observed in repeated tests; thus, they are not by themselves indicative of differences in the physics of accretion from Appendix C to SLD.

For a velocity of 200 kt at a stagnation freezing fraction of 0.30 (11 (b)), the horns for the SLD and Appendix C cases varied slightly in position, but showed no particular trend with drop size. The quantity of ice formed in the main accretion also appeared to be much the same for each drop *MVD*. The variations again appeared to be no more significant than typical run-to-run deviations.

Figures 11 (c) and (d) compare profiles generated for a range of *MVD*s at $n_0 = 0.50$. Main ice shapes and sizes for 30, 115 and 165 μm matched well at a velocity of 100 kt (11 (c)). For a velocity of 200 kt (11 (d)), the three shapes had the same leading-edge thickness, because the product $\beta_0 A_c$ for all 3 *MVD*s was the same. In addition, horn locations and horn angle agreed well for the three. However, because $\beta_0$ was not maintained constant, more ice was accreted on the aft surfaces of the SLD horns than for those of the 30-μm *MVD*. The size of the feathers also increased with drop size.

The largest model tested had a chord of 183 cm. Ice profiles resulting from varying the *MVD* for this model are presented in figure 12. Figures 12 (a) and (b) show ice shapes for a stagnation freezing fraction of 0.30. The shapes in figure 12 (a) were generated at a velocity of 100 kt, and those in 12 (b) at $V = 200$ kt.

In figure 12 (a), ice-shape profiles for *MVD*s of 30, 85 and 170 μm are reproduced. While the SLD (85- and 170-μm) accretions matched in both shape and size, the Appendix C (30-μm) result was significantly different in shape and appeared to be somewhat smaller in size from the others. At 200 kt (12 (b)), ice shapes for *MVD*s of 30 and 135 μm were of similar appearance, although the horn angles and total size of the accretions were not perfect matches.

Figures 12 (c) and (d) compare ice shapes obtained at a stagnation freezing fraction of 0.50 and velocities of 100 kt (12 (c)) and 200 kt (12 (d)). At 100-kt, the SLD (85- and 170-μm) main ice shapes were nearly identical in shape and size. However, both were significantly smaller than the Appendix C (30-μm) accretion. The SLD feathers were significantly larger than those of the Appendix C encounter. Of all the examples presented in figures 10, 11 and 12, this is the only instance for which the SLD main accretions were smaller than the Appendix C.

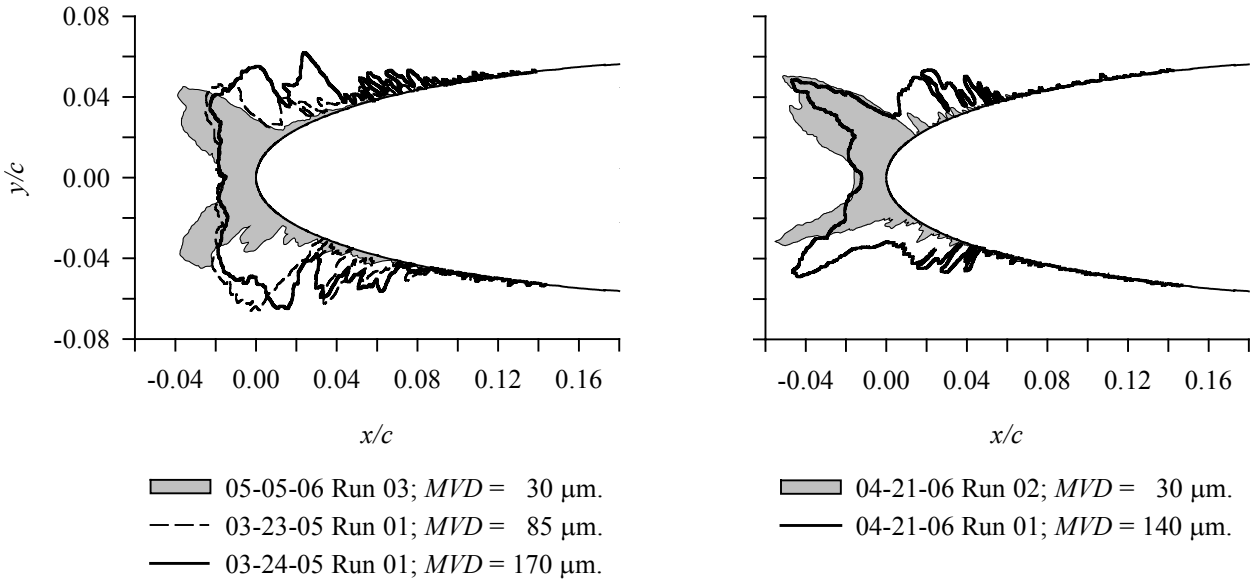


(a) $V$, 100 kt; $n_0$, 0.30.

(b) $V$, 200 kt; $n_0$, 0.30.

| | Date/Run | $c$, cm | $t_{st}$, °C | $t_{tot}$, °C | $V$, kt | $MVD$, μm | $LWC$, g/m$^3$ | $\tau$, min | $\beta_0$, % | $A_c$ | $\beta_0 A_c$ | $n_0$ | $We_\delta$, $10^3$ | $We_L$, $10^6$ |
|---|---|---|---|---|---|---|---|---|---|---|---|---|---|---|
| (a) | 05-05-06/03 | 182.9 | -10 | -9 | 99 | 30 | 1.75 | 32.5 | 54.7 | 3.28 | 1.80 | 0.30 | 1.2 | 2.31 |
| | 03-23-05/01 | 182.9 | -10 | -8 | 100 | 85 | 0.96 | 36.7 | 83.3 | 2.05 | 1.70 | 0.31 | 3.4 | 2.34 |
| | 03-24-05/01 | 182.9 | -12 | -11 | 100 | 170 | 1.45 | 22.9 | 92.3 | 1.93 | 1.78 | 0.30 | 6.9 | 2.35 |
| (b) | 04-21-06/02 | 182.9 | -13 | -8 | 199 | 30 | 1.10 | 22.0 | 63.8 | 2.81 | 1.80 | 0.30 | 4.8 | 9.36 |
| | 04-21-06/01 | 182.9 | -9 | -4 | 200 | 140 | 0.40 | 41.8 | 92.7 | 1.95 | 1.80 | 0.30 | 22.7 | 9.39 |

**Figure 12**. Effect of Drop Size on Ice Shape for a Chord of 182.9 cm.

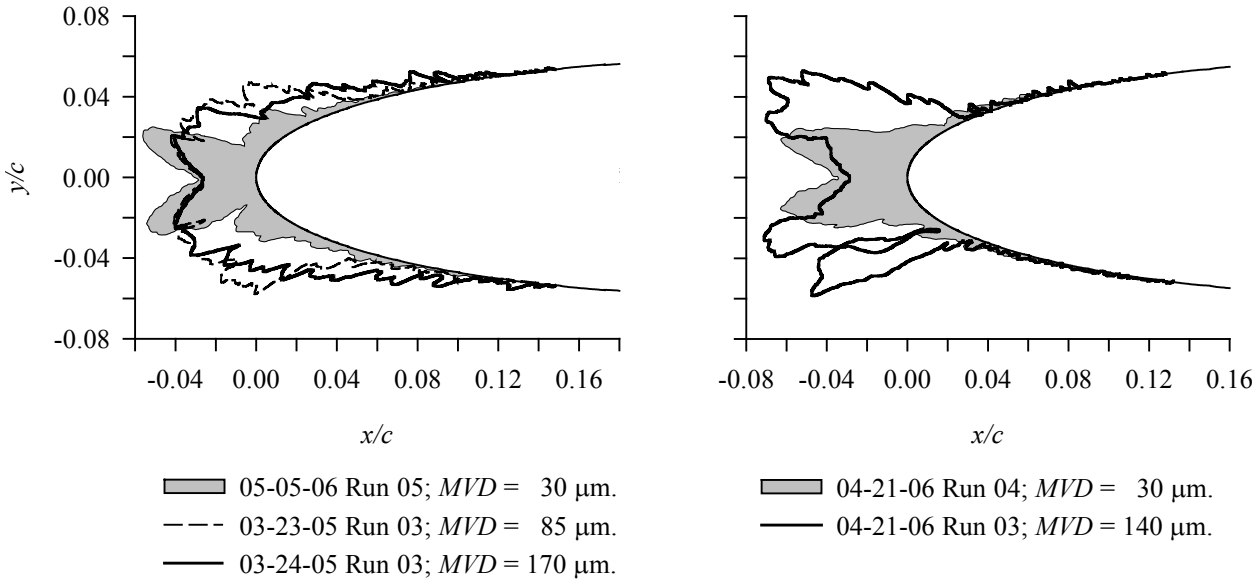


(c) $V$, 100 kt; $n_0$, 0.50.

(d) $V$, 200 kt; $n_0$, 0.50.

| | Date/Run | $c$, cm | $t_{st}$, °C | $t_{tot}$, °C | $V$, kt | $MVD$, μm | $LWC$, g/m$^3$ | $\tau$, min | $\beta_0$, % | $A_c$ | $\beta_0 A_c$ | $n_0$ | $We_{\delta}$, $10^3$ | $We_L$, $10^6$ |
|---|---|---|---|---|---|---|---|---|---|---|---|---|---|---|
| (c) | 05-05-06/05 | 182.9 | -17 | -16 | 100 | 30 | 1.74 | 32.5 | 54.9 | 3.29 | 1.80 | 0.50 | 1.2 | 2.33 |
| | 03-23-05/03 | 182.9 | -16 | -15 | 100 | 85 | 0.96 | 36.7 | 83.3 | 2.06 | 1.72 | 0.52 | 3.5 | 2.37 |
| | 03-24-05/03 | 182.9 | -21 | -20 | 100 | 170 | 1.45 | 22.9 | 92.3 | 1.93 | 1.78 | 0.50 | 6.9 | 2.35 |
| (d) | 04-21-06/04 | 182.9 | -20 | -15 | 199 | 30 | 1.10 | 22.0 | 64.0 | 2.82 | 1.80 | 0.50 | 4.9 | 9.35 |
| | 04-21-06/03 | 182.9 | -14 | -9 | 200 | 140 | 0.40 | 41.8 | 92.7 | 1.95 | 1.80 | 0.50 | 22.8 | 9.40 |

**Figure 12**. (con't).

At 200 kt (fig. 12 (d)), only one SLD condition, with an *MVD* of 140 μm, was tested. For this SLD case, the feathers have merged sufficiently with the main ice shape to make it difficult to distinguish the two regions. However, there appears to be little similarity between either the shapes or the size of the SLD and Appendix C accretions. Further examination of the videos taken of the SLD icing process during accretion and photos taken after the completion of the spray show that many large feathers were formed quickly along the test model centerline region likely due to the poor uniformity of this SLD cloud, and then those feather structures distorted the way the main ice shape grew. Additional studies are needed in understanding the potential causes of large feather formation other than unique physics of SLD icing for scaling test

One final set of comparisons for the 183-cm-chord model is presented in figures 12 (e) and (f). For these tests, the velocity was 150 kt, and profiles for 30, 110 and 190 μm are shown. The stagnation freezing fractions were 0.30 for the results shown in figure 12 (e) and 0.50 for 12 (f). The agreement between the Appendix C and SLD main ice shapes was fairly good for both freezing fractions, although the SLD tests produced significantly larger feathers than the Appendix C. While it appears that the SLD main shapes are larger than those for Appendix C, this may be an illusion created by large feathers adjacent to the main ice shape. Experience with this model is too limited to draw conclusions.

Earlier in this paper, it was demonstrated that with constant $n_0$, changes in either model size or velocity affected horn angle and location. Changes in *LWC*, however, had no effect as long as temperature was modified to maintain $n_0$. Figures 10, 11, and 12 have now shown, with a few exceptions, that *MVD* over the range 30 to 190 μm also had no effect on horn angle and location. Greater horn thickness for SLD cases compared with

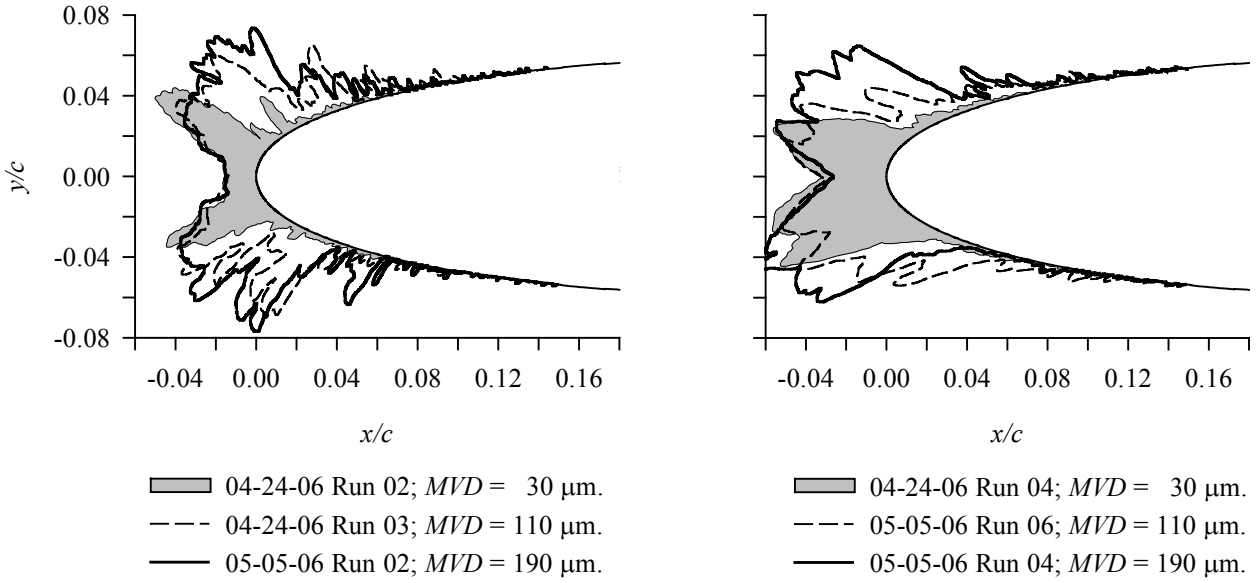


(e) $V$, 150 kt; $n_0$, 0.30.

(f) $V$, 150 kt; $n_0$, 0.50.

| | Date/Run | $c$, cm | $t_{st}$, °C | $t_{tot}$, °C | $V$, kt | $MVD$, μm | $LWC$, g/m$^3$ | $\tau$, min | $\beta_0$, % | $A_c$ | $\beta_0 A_c$ | $n_0$ | $We_\delta$, $10^3$ | $We_L$, $10^6$ |
|---|---|---|---|---|---|---|---|---|---|---|---|---|---|---|
| (e) | 04-24-06/02 | 182.9 | -11 | -9 | 150 | 30 | 1.34 | 25.5 | 60.3 | 2.98 | 1.80 | 0.30 | 2.7 | 5.27 |
| | 04-24-06/03 | 182.9 | -12 | -9 | 150 | 110 | 0.94 | 24.8 | 89.3 | 2.04 | 1.82 | 0.30 | 10.0 | 5.28 |
| | 05-05-06/02 | 182.9 | -11 | -8 | 150 | 190 | 0.73 | 30.0 | 94.2 | 1.91 | 1.80 | 0.30 | 17.3 | 5.26 |
| (f) | 04-24-06/04 | 182.9 | -19 | -16 | 149 | 30 | 1.34 | 25.5 | 60.3 | 2.98 | 1.80 | 0.50 | 2.7 | 5.25 |
| | 05-05-06/06 | 182.9 | -19 | -16 | 150 | 110 | 0.94 | 24.8 | 89.3 | 2.04 | 1.82 | 0.49 | 10.1 | 5.29 |
| | 05-05-06/04 | 182.9 | -17 | -14 | 151 | 190 | 0.73 | 30.0 | 94.2 | 1.92 | 1.81 | 0.50 | 17.6 | 5.34 |

**Figure 12**. (concluded).

Appendix C can likely be attributed to higher collection efficiencies aft of the leading edge, rather than to any fundamental differences in ice accretion physics between the two drop-size regimes. This lack of an *MVD* effect means that for the conditions studied here, new similarity parameters do not appear to be necessary to conduct a scaling analysis for SLD conditions. Consequently, the same scaling methods used for Appendix C clouds should apply. Figure 2 showed that when $\beta_0$ is matched these differences should be eliminated.

Unlike the similarities between Appendix C and SLD main ice shapes, feather formations in the SLD regime seen in figures 10, 11 and 12 were often significantly larger than those in Appendix C. But these differences may also have been the result of significantly higher collection efficiencies aft of the main ice shape for the SLD tests. Feather accretion is not well understood and more study of this region is needed before conclusions can be made.

Most of the experimental examples above suggest that SLD icing probably does not involve physical phenomena different from Appendix C. To see if this thesis is supported by the LEWICE ice-accretion code[14,15] LEWICE 3.2 was run with the splashing module turned off. Figure 13 compares the predicted ice accretions for *MVD*s of 30, 120 and 200 μm on a 27-cm-chord NACA 0012 at an angle of attack of 0°, a velocity of 200 kt and a stagnation freezing fraction of 0.50. The conditions for the 30-μm cloud were those shown in the table for figure 10 (b) (08-28-04 run 3). Conditions for the 120- and 200-μm clouds were adjusted to maintain a stagnation freezing fraction of 0.50 and with the icing time varied such that the product $\beta_0 A_c$ was the same for all three *MVD*s. This is the same way conditions were modified for each of the experimental comparisons shown in figures 10 to 12. All three LEWICE runs used a monodisperse drop distribution. The LEWICE ice-shapes in figure 13 were nearly identical, indicating no

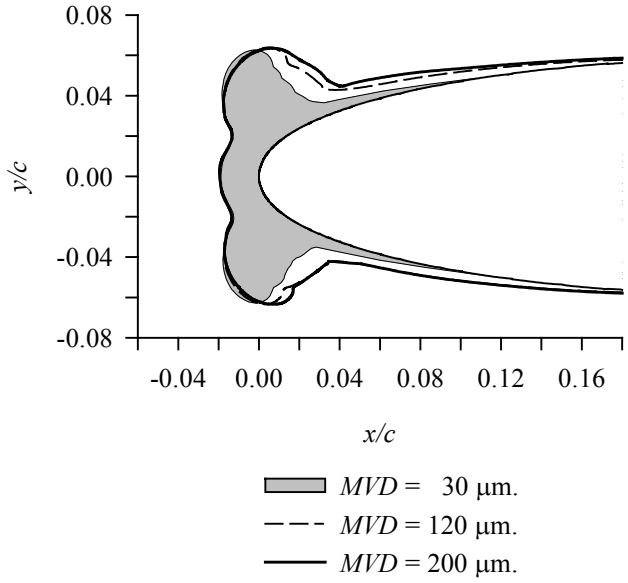


**Figure 13.** LEWICE 3.2[28] Predictions of Effect of *MVD*. *c*, 27 cm; *V*, 200 kt; $n_0$, 0.50. Monodisperse Drop-Size Distributions.

effect of *MVD*. The main ice shapes were nearly the same size and form, although the SLD drop sizes produced slightly larger accumulations downstream of the forward face. This lack of an *MVD* effect for the main ice shape is consistent with the experimental results. However, its effect on ice mass is not known at this time since mass has not been measured in the scaling experiments report here.

Direct comparisons of LEWICE predictions with experimental accretions are shown in figure 14 for a monodisperse drop size of 190 μm. The LEWICE 3.2 optional splashing module was again turned off for these calculations. Nevertheless, the main ice profiles agreed with experimental sizes and shapes for stagnation freezing fractions of both 0.30 (fig. 14 (a)) and 0.50 (fig. 14 (b)). Aft of the main accretion discrete feather formations are apparent in the experimental profiles. LEWICE lacks a model for feather growth and consequently predicts a continuous accretion in both the main ice shape and the feather region. For this reason, it is not valid to compare experimental feather formations with either LEWICE shapes or quantities in the feather region.

Based on photographic evidence[32], there can be no doubt that splashing at the leading edge of an airfoil occurs in icing conditions. However, the experimental ice shape profiles presented here tell us that these splashing events apparently do not influence the main ice shape in any significant way. An understanding of the physics of formation in the feather region is needed, but studies to date have not been adequate to develop a good model.

Because of the absence of significant *MVD* effects on the main ice shape, methods used to scale model size for Appendix C conditions should also work equally well for SLD conditions, at least up to about 190 μm, the maximum value of existing experimental evidence. These scaling methods are limited to scaling the main ice accretion, with no attempt to model the feather region. While it is possible that scaling of the feather region may need to be handled as a separate issue once the physics of feather formation is better understood, the scaling method described in this paper appears to scale both the main and feather regions adequately. This issue will be discussed later in the section Recommended Scaling Methods.

LWC

Figure 2 illustrated the strong effect freezing fraction has on ice shape. Because of this importance, Olsen and Newton[4] proposed a scaling method in which only scale and reference $n_0$ along with $A_c$ would be matched. This method is not adequate when model size is scaled, but to scale *LWC* with full-size models the Olsen method is an effective approach. Typically, this method is applied in situations for which scale and reference *V* and *MVD* can be matched, as well as the model size. Reference 2 showed that if temperature was adjusted to keep $n_0$ constant, ice shapes remained essentially unchanged when *LWC* was nearly doubled for Appendix C drop sizes.

Figure 15 shows examples of tests performed to validate the Olsen method over a wider range of *LWC*. Figure 15 (a) compares shapes for *LWC* varied from 0.58 to 2.19 g/m$^3$ with Appendix C drop sizes. To perform these tests it was necessary to use both nozzle types currently available in the IRT: Mod-1 nozzles for the lower value of *LWC* and Standard for the higher. The tests were made with spray-bar conditions based on the then-current calibration, which indicated an *MVD* of 30 μm for each test. However, the latest interpretation of calibration data suggests somewhat different *MVD*s for the two tests, as shown in the table accompanying figure 15. Nevertheless, the agreement of the two ice shapes is very good.

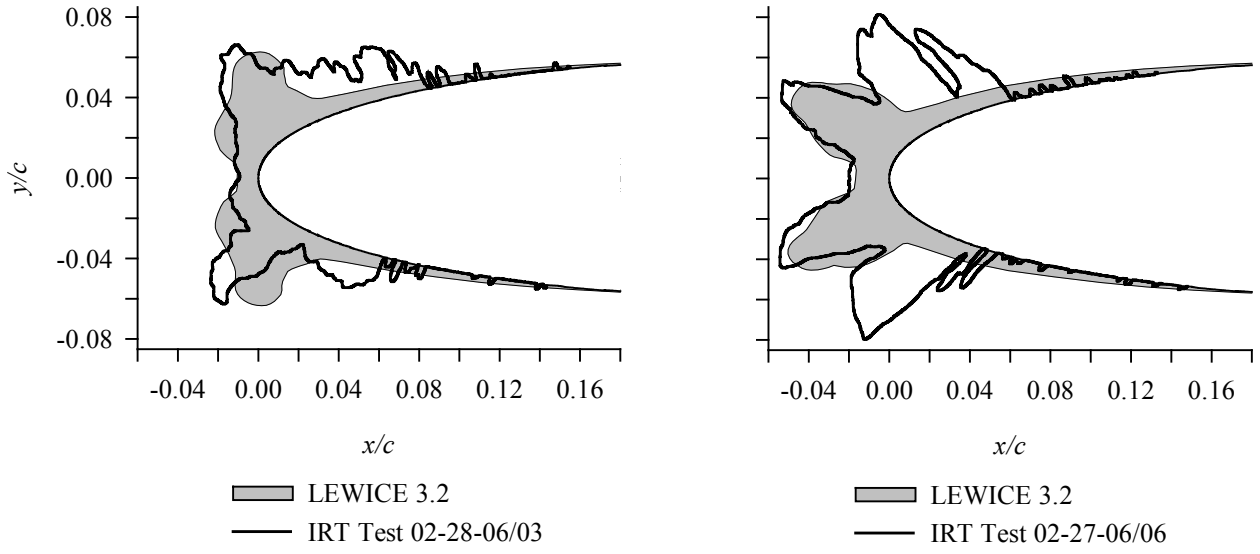


(a) $n_0$, 0.30. (b) $n_0$, 0.50.

**Figure 14.** LEWICE 3.2[28] Predictions Compared with Experimental Ice Shape for SLD. $c$, 91 cm; $V$, 200 kt; $MVD$, 190 μm with Monodisperse Drop-Size Distributions. See figures 11 (b) and (d) for complete test conditions.

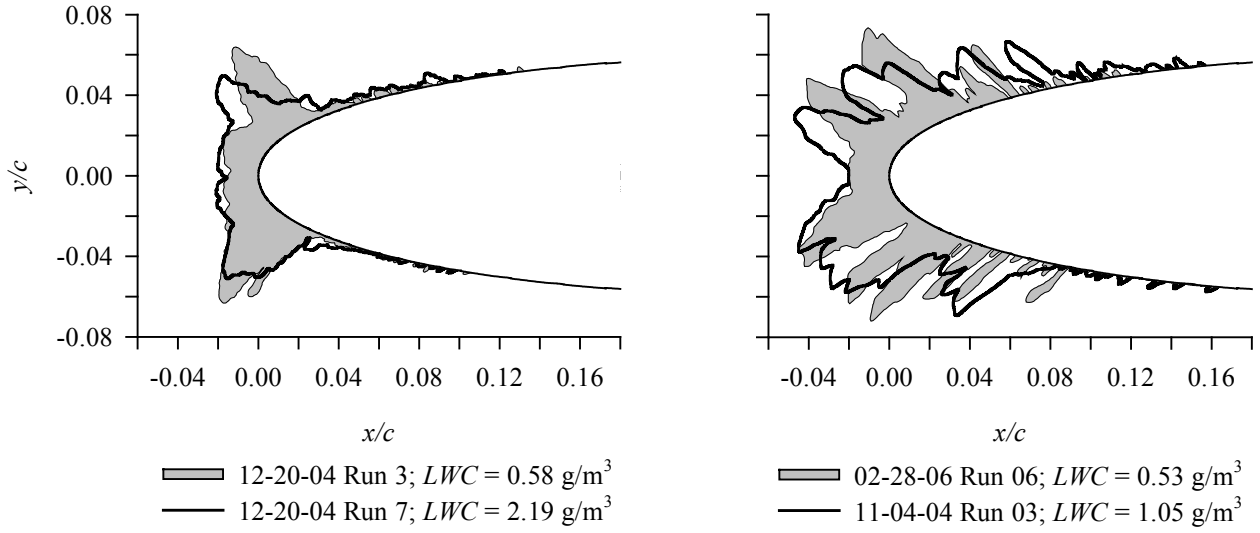


(a) Appendix C. (b) SLD.

| | Date/Run | $c$, cm | $t_{st}$, °C | $t_{tot}$, °C | $V$, kt | $MVD$, μm | $LWC$, g/m$^3$ | $\tau$, min | $\beta_0$, % | $A_c$ | $\beta_0 A_c$ | $n_0$ | $We_\delta$, $10^3$ | $We_L$, $10^6$ |
|---|---|---|---|---|---|---|---|---|---|---|---|---|---|---|
| (a) | 12-20-04/03 | 91.4 | -6 | -3 | 150 | 26 | 0.58 | 28.2 | 69.6 | 2.85 | 1.99 | 0.28 | 2.4 | 2.64 |
| | 12-20-04/07 | 91.4 | -13 | -10 | 150 | 33 | 2.19 | 7.1 | 75.8 | 2.71 | 2.06 | 0.28 | 3.0 | 2.63 |
| (b) | 02-28-06/06 | 91.4 | -11 | -8 | 150 | 115 | 0.53 | 20.7 | 94.0 | 1.92 | 1.80 | 0.50 | 10.5 | 2.64 |
| | 11-04-04/03 | 91.4 | -17 | -14 | 150 | 117 | 1.05 | 10.3 | 94.2 | 1.89 | 1.78 | 0.49 | 10.7 | 2.64 |

**Figure 15**. Effect of Varying $LWC$ with Constant Stagnation freezing fraction.

Figure 15 (b) makes a comparison for SLD conditions for *LWC*s of 0.53 and 1.05 g/m$^3$. The values of *LWC* available for testing with SLD *MVD*s in the IRT are limited at the present by the calibration that has been completed, so it is not possible to demonstrate the Olsen method over a larger range of *LWC*s.

Both tests used Mod-1 nozzles. Although the profiles are not in perfect conformity, the leading-edge thickness and horn angles are in good agreement. The most noticeable difference was that the accretion of 02-28-06 exhibited a flat region between the horns near stagnation. For the 11-04-04 accretion, the base of the horns met in a V. A nozzle air pressure of 2.5 psig was required for the 2006 tests, while the 2004 tests used a pressure of 5 psig. Thus, one possibility that needs more study is that characteristics of the two SLD clouds may have differed. Until further tests are made, however, we do not know if the shape difference is significant.

The large feathers aft of the main ice shape agreed in angle and size for the two tests in figure 15 (b), although the positions did not. However, the differences apparent in both main ice accretion and feathers do not appear to be significantly greater than those often seen with repeated tests. Thus, the comparisons of figure 15 confirm that the Olsen method can be used to scale *LWC* over at least a limited range for both Appendix C and SLD conditions.

These results also have implications for model-size scaling. In the Ruff method[2,3], the scale *LWC* is found by matching scale and reference stagnation freezing fraction from equations (7) – (10) after first establishing scale temperature by matching the water energy transfer parameter, equation (8). But the Olsen scaling results suggest that the value of *LWC* is not so important by itself, as long as the freezing fraction is matched. This principle can also be applied to scaling involving reduced-size models by allowing the scale *LWC* to be chosen arbitrarily. Similarly, it was also shown earlier in this study that the value of *MVD,* over the range 30 to 190 μm, appears to have no significant effect on the main ice shape provided $n_0$ and $\beta_0 A_c$ are matched. This lack of an *MVD* effect can also let *MVD* be selected somewhat arbitrarily. For tunnels without altitude simulation capability, once the scale *LWC* is picked, the remaining scale test conditions (temperature, velocity, *MVD* and time) can be determined by matching at most four similarity parameters in the manner described in the following section Recommended Scaling Methods.

Icing Limits

Icing limit data for NACA 0012 models with chords of 53.3 and 91.4 cm have been presented by Anderson and Tsao[37]. These data showed a strong correlation with $\beta_0$ only. Since then, additional icing limits have been recorded for models ranging from 26.7 to 182.9 cm. Icing limits were established by noting the chord-wise position on the model at which ice accretion (in the form of feathers) appeared to end. Ice shapes were traced once at the span-wise centerline and again 2.5 cm above that center (the models were mounted vertically in the IRT). For each of these ice-shape profiles an icing limit was estimated on both the upper and the lower surface. Because the models were mounted at 0° AOA, the upper- and lower-surface limits can reasonably be expected to be the same, within some random variation. Values for the two tracing locations should also vary little. Therefore, the four values of icing limit were averaged to obtain a single limit for each test.

These average icing limits obtained over the period 2002 to 2006 are presented in Figure 16 normalized by chord and plotted as a function of the stagnation collection efficiency. Data for each of the 5 chords tested are given with a different symbol. The solid line represents a simple least-squares curve fit through all of the data. The fit was forced to pass through the origin. The data scatter in location, $x/c$, about this line is typically ±0.05. The results show a strong correlation with $\beta_0$ and an independence of model size. Attempts to correlate the data with either $V$ or $n_0$ were not successful.

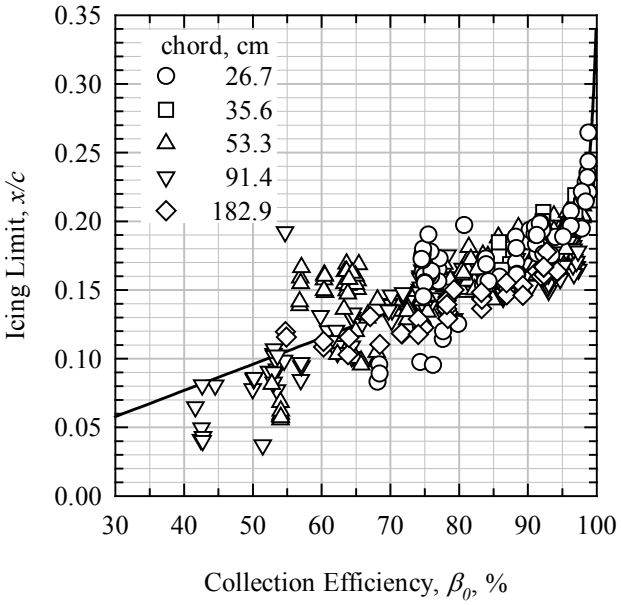


**Figure 16.** Icing Limits Recorded in IRT Scaling Tests. NACA 0012 Models at 0° AOA.

Recommended Scaling Methods

The preceding sections demonstrated that the effects of model size, velocity, *MVD* and *LWC* are no different for the SLD conditions reviewed than for Appendix C conditions, with the possible exception of an *MVD* effect for the 183-cm-chord model at a velocity of 200 kt (fig. 12 (d)). These effects are being considered when developing recommended scaling methods for model-size scaling, test-condition scaling as well as icing-limit scaling. They can be summarized as follows: (1) An increase in model size as measured by chord causes the included horn angle of the main ice shape to decrease. Therefore, testing with a reduced-size model requires the application of scaling methods. (2) As $V$ increases, the included horn angle of the main ice shape tends to decrease. This effect can be accounted for through the similarity parameter $We_L$. (3) *MVD* for the range 30 to 190 μm appears to have no strong effect on the main ice shape provided $n_0$ and $\beta_0 A_c$ are matched with constant velocity and model size. While it is desirable to match scale and reference values of $\beta_0$, this parameter does not have to be matched precisely for good success in scaling the main ice shape. Therefore, the choice of *MVD* can be somewhat flexible and a fairly close match (within 10%) is suggested. However, to match to scale icing limits a good match of $\beta_0$ is required. A good method to scale feather structures has not yet been developed. (4) Increasing $n_0$ has the effect of increasing the stagnation thickness while decreasing the included horn angle of the main ice shape. *LWC* appears to have no effect independent of $n_0$. Consequently, scale *LWC* values can be chosen somewhat arbitrarily to suit facility capabilities. (5) Selection of the correct accretion time is, of course, important to obtaining the right amount of ice. Therefore, the accumulation parameter $A_c$ must be included in scaling methods. When $\beta_0$ has not been matched, the combination $\beta_0 A_c$ must be matched to obtain the correct quantity of ice in the main accretion.

Scaling of Main Ice Shape for Reduced Model Size

These observations indicate that for *MVD* up to 190 μm, SLD scaling methods need be no different from those used for Appendix C conditions. The method used in reference 2 will therefore be recommended for SLD. This procedure for model-size scaling will be outlined here and followed by results of icing scaling tests.

1. Calculate reference similarity parameters $A_c$, $\beta_0$, and $n_0$ from equations (1), (2) – (6), and (7) – (10), respectively.

2. Select scale velocity by matching scale and reference $We_L$. From equation (12) this leads to

$$V_S = V_R \sqrt{\frac{c_R}{c_S}}$$

3. Knowing $V_S$, find the scale *MVD* that satisfies the equation $\beta_{0,S} = \beta_{0,R}$. If $MVD_S$ so found is less than 25 μm, set $MVD_S$ to a value between 25 and 30 μm. Although smaller scale *MVD*s may provide acceptable scale ice shapes, the method used here has not yet been tested for scale drop sizes below 25 μm. If the scale *MVD* is outside the low end of the facility calibration range, set $MVD_S$ to 30 μm. Furthermore, if facility restrictions on *MVD* make it impractical to match $\beta_0$ exactly, scale *MVD* should be selected to gain as close a match of $\beta_0$ as possible.

4. Choose a convenient $LWC_S$.

5. Calculate the scale static temperature $t_{st,S}$ that satisfies $n_{0,S} = n_{0,R}$.

6. Calculate the scale total temperature, $t_{tot,S}$. Reference 2 reported that total temperatures near freezing can produce highly non-repeatable ice shapes. Therefore, if $t_{tot,S}$ is greater than -2°C, repeat steps 4, 5 and 6 with a larger $LWC_S$.

7. If $\beta_{0,S} = \beta_{0,R}$, calculate the scale accretion time, $\tau_S$, by matching scale and reference $A_c$. If $\beta_{0,S} \neq \beta_{0,R}$, calculate the scale accretion time, $\tau_S$, by matching scale and reference $\beta_0 A_c$.

The scaling method outlined above was evaluated in reference 2 for Appendix C conditions and the experimental examples provided would not be repeated here. Additional scaling tests with SLD reference conditions have now been performed using this method as well. Several NACA 0012 models up to 183-cm chord, reference velocities of 100, 150 and 200 kt, reference *MVD*s up to 190 μm and scale *MVD*s of approximately 30 μm were used.

Figures 17 through 19 show results of tests to scale ice shape by applying the above method. These examples demonstrate how the ice shapes produced by reference tests with *MVD*s in the SLD regime can be simulated by tests using scale models operated in Appendix C conditions. Ice-shape profiles will be compared for freezing fractions of both 0.30 and 0.50 for each of the scaling scenarios.

In figure 17, examples are given of scaling with a model-size ratio of 2.6 (scaling from 91.4-cm chord to 35.6-cm), a reference velocity of 200 kt and a reference *MVD* of 115 μm. The scale test conditions gave a match

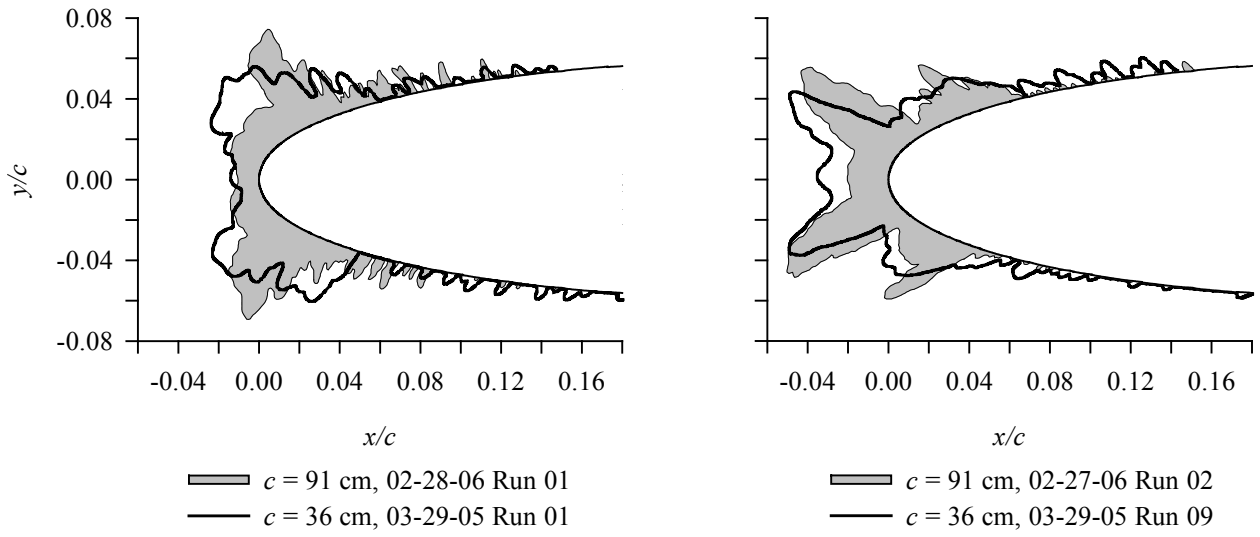


(a) $n_0$, 0.30.

(b) $n_0$, 0.50.

| | Date/Run | $c$, cm | $t_{st}$, °C | $t_{tot}$, °C | $V$, kt | $MVD$, μm | $LWC$, g/m$^3$ | $\tau$, min | $\beta_0$, % | $A_c$ | $\beta_0 A_c$ | $n_0$ | $We_\delta$, $10^3$ | $We_L$, $10^6$ |
|---|---|---|---|---|---|---|---|---|---|---|---|---|---|---|
| (a) | 02-28-06/01 | 91.4 | -8 | -2 | 200 | 115 | 0.37 | 22.7 | 94.7 | 1.95 | 1.85 | 0.29 | 18.6 | 4.68 |
| | 03-29-05/01 | 35.6 | -12 | 0 | 297 | 37 | 0.57 | 4.3 | 92.2 | 2.18 | 2.01 | 0.26 | 13.4 | 4.02 |
| (b) | 02-27-06/02 | 91.4 | -11 | -6 | 200 | 115 | 0.37 | 22.8 | 94.7 | 1.96 | 1.86 | 0.49 | 18.6 | 4.68 |
| | 03-29-05/09 | 35.6 | -16 | -4 | 295 | 37 | 0.57 | 4.3 | 92.1 | 2.18 | 2.01 | 0.46 | 13.3 | 3.99 |

**Figure 17**. Scaling from 91- to 36-cm-Chord using Constant-$We_L$ Method. $V_R$, 200 kt; $MVD_R$, 115 μm.

of the reference parameters $\beta_0$, $\beta_0 A_c$ and $n_0$ within 10%. Scale and reference $We_L$ agreed only within 17%. The accretion profiles in figure 17 (a) ($n_0$ approximately 0.3) displayed some differences between the scale and reference horn locations. However, the total temperature for the scale test (03-29-05 run 01) was near 0°C, and reference 2 noted that ice accretions produced with total temperatures near freezing cannot be relied upon for consistent and repeatable shapes. When planning scale tests it is important to remember that scale $LWC$s should be chosen to permit a match of $n_0$ with total temperatures 2°C or more below freezing.

The tests represented in figure 17 (b) were made with much the same conditions as 17 (a), but with lower temperatures to provide a freezing fraction near 0.5. The scale horns were not spread as far apart as those on the reference accretion, but the general size and angle were simulated fairly well. The sizes of the feathers aft of the main shape were also simulated well by the scale test.

Figure 18 shows examples of scaling for a reference-to-scale model-size ratio of 6.9 (182.9-cm to 26.7-cm chord). The reference velocity for these tests was 100 kt and the reference $MVD$ was 170 μm. The scale and reference parameters $\beta_0$, $\beta_0 A_c$ and $n_0$ were in close agreement, while $We_L$ matched to approximately 11%.

Main ice shapes and feather regions of the scale tests simulated the reference profiles well for both freezing fractions. These results show that the scaling method recommended here can be applied to fairly large model chords as well as to SLD conditions. Higher reference velocities for this model-size ratio were not tested because the resulting necessary scale velocities become too high. For example, for a model-size ratio of 6.9 and a reference velocity of 150 kt, the scale velocity to permit matching of $We_L$ is nearly 400 kt. The maximum empty-test-section velocity in the IRT is 350 kt. Furthermore, as speed increases above about 300 kt, shedding of both main ice accretions and feathers, particularly at low freezing fractions, leads to questionable scale results.

Reference velocities higher than 100 kt were tested with the 183-cm-chord NACA 0012 model, but with the reference-to-scale model-size ratio reduced. Instances

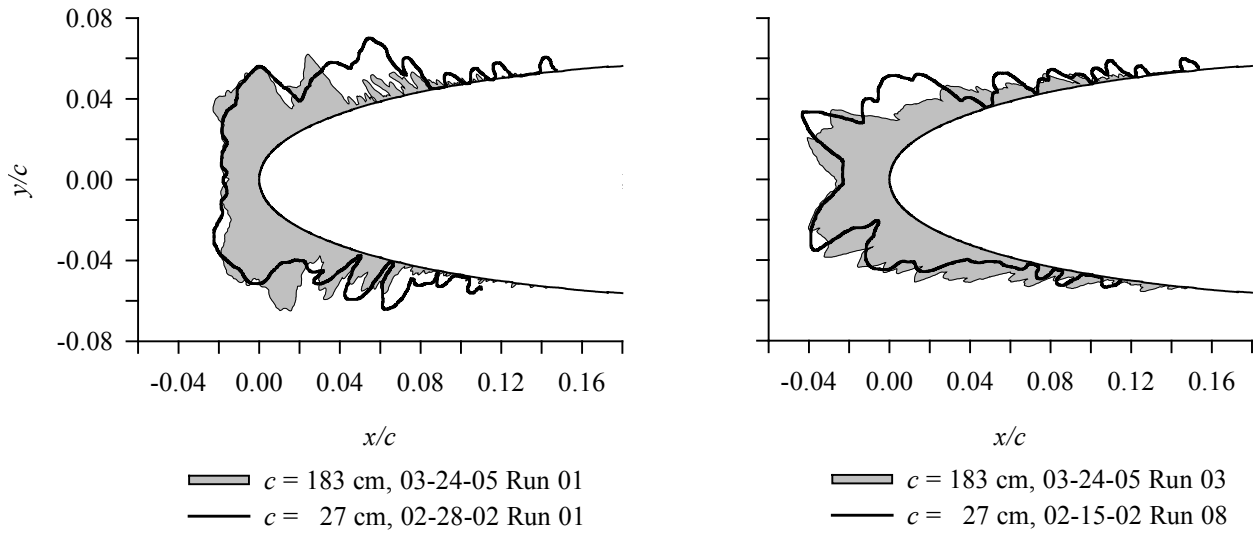


(a) $n_0$, 0.30.

(b) $n_0$, 0.50.

| | Date/Run | $c$, cm | $t_{st}$, °C | $t_{tot}$, °C | $V$, kt | $MVD$, μm | $LWC$, g/m$^3$ | $\tau$, min | $\beta_0$, % | $A_c$ | $\beta_0 A_c$ | $n_0$ | $We_\delta$, $10^3$ | $We_L$, $10^6$ |
|---|---|---|---|---|---|---|---|---|---|---|---|---|---|---|
| (a) | 03-24-05/01 | 182.9 | -12 | -11 | 100 | 170 | 1.45 | 22.9 | 92.3 | 1.93 | 1.78 | 0.30 | 6.90 | 2.35 |
| | 02-28-02/01 | 26.7 | -12 | -2 | 268 | 33 | 0.86 | 2.1 | 92.3 | 1.94 | 1.79 | 0.30 | 9.59 | 2.47 |
| (b) | 03-24-05/03 | 182.9 | -21 | -20 | 100 | 170 | 1.45 | 22.9 | 92.2 | 1.93 | 1.78 | 0.50 | 6.90 | 2.35 |
| | 02-15-02/08 | 26.7 | -15 | -5 | 276 | 31 | 0.64 | 2.7 | 92.0 | 1.89 | 1.74 | 0.50 | 9.71 | 2.61 |

**Figure 18**. Scaling from 183- to 27-cm-Chord using Constant-$We_L$ Method. $V_R$, 100 kt; $MVD_R$, 170 μm.

of scaling to a 53-cm-chord model with a 150-kt reference velocity are shown in Figure 19. Figures 19 (a) and (b) show results for a freezing fraction of 0.3, while 19 (c) and (d) are for a freezing fraction of 0.5. Tests were made with reference *MVD*s of 110 (fig. 19 (a) and (c)) and 190 μm (fig. 19 (b) and (d)). In each case, there was a close match of $\beta_0 A_c$, $n_0$ and $We_L$, but with a scale *MVD* of 30 μm, $\beta_0$ was not always well matched to the reference.

The main ice shape size and horn angles of the reference tests were matched well in the scale tests in each case. However, the reference tests produced large feather structures just aft of the main shape that were not seen in the 100-kt reference accretions of figure 18. These feather structures became more prominent when the *MVD* was increased from 110 to 190 μm.

Methods to simulate these large feathers in scale tests have not yet been developed, and studies of feather formation are in early stages[23,24]. There is no evidence in the results to date, however, to suggest that feathers form differently in the SLD regime than they do in Appendix C. The present belief is that the large feather structures seen in SLD at velocities higher than 100 kt is simply a result of the higher collection efficiencies at these conditions. Note in the results of Figure 19 that the better the match of $\beta_0$ between scale and reference, the better the match between the scale and reference aft feather size.

Further tests are needed to demonstrate scaling from the 183-cm model at 200-kt reference velocity. To avoid an excessive scale velocity the scale model for these tests should be no smaller than half the reference size.

Scaling of Icing Limit

Above discussions have shown that, although highly desirable, $\beta_0$ does not have to be matched exactly for good scaling of the main ice shape; therefore, the choice of *MVD* can be somewhat flexible. However, to simulate feather growth, it is probably important that scale and reference $\beta_0$ not differ by much. In addition, if icing limits are important to the scaled test objective, figure 16 shows that scale $\beta_0$ should be matched to the reference value. If both main ice shape and icing limits are required to be scaled and facility restrictions on *MVD* make it impractical to match $\beta_0$ exactly to find the

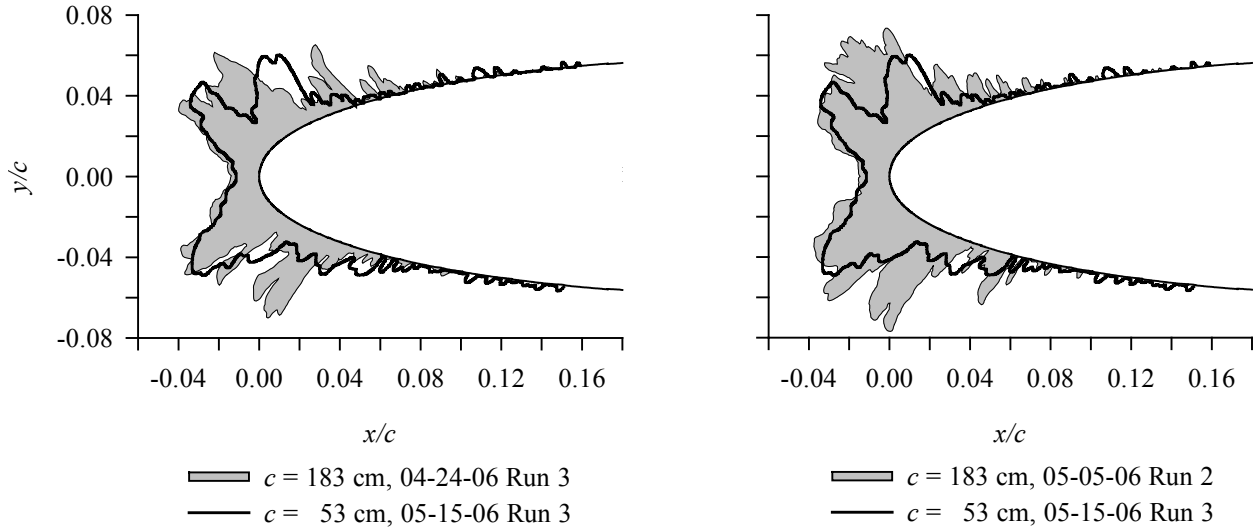


(a) *MVD*, 110 μm; $n_0$, 0.30.

(b) *MVD*, 190 μm; $n_0$, 0.30.

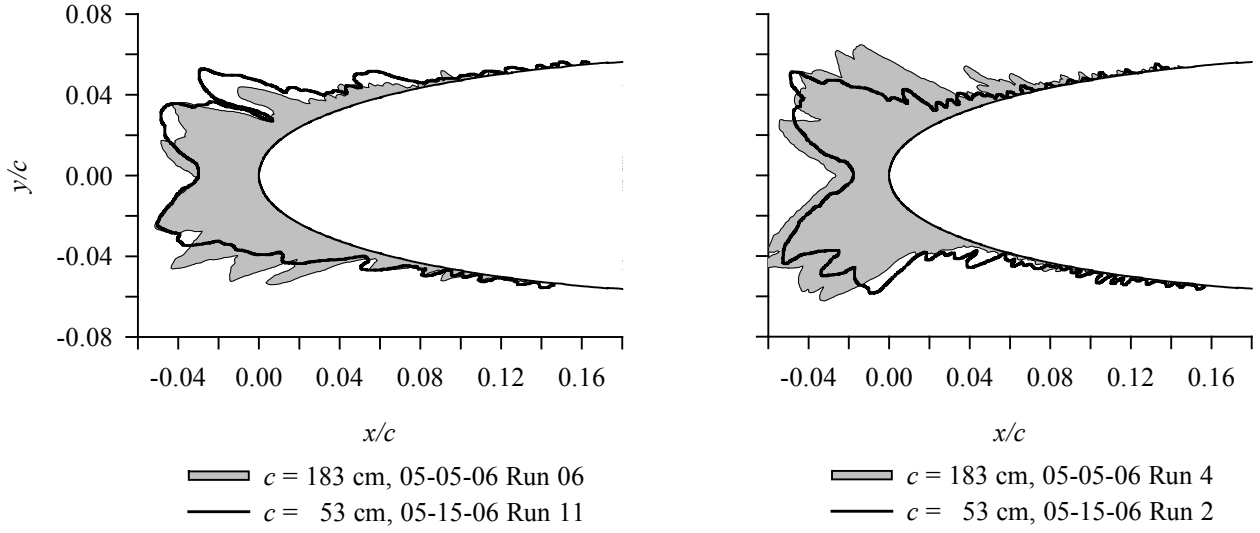


(c) $MVD_R$, 110 μm; $n_0$, 0.50.

(d) $MVD_R$, 190 μm; $n_0$, 0.50.

| | Date/Run | $c$, cm | $t_{st}$, °C | $t_{tot}$, °C | $V$, kt | $MVD$, μm | $LWC$, g/m$^3$ | $\tau$, min | $\beta_0$, % | $A_c$ | $\beta_0 A_c$ | $n_0$ | $We_\delta$, $10^3$ | $We_L$, $10^6$ |
|---|---|---|---|---|---|---|---|---|---|---|---|---|---|---|
| (a) | 04-24-06/03 | 182.9 | -12 | -9 | 150 | 110 | 0.94 | 24.8 | 89.2 | 2.03 | 1.81 | 0.30 | 10.0 | 5.28 |
| | 05-15-06/03 | 53.3 | -13 | -3 | 277 | 30 | 0.84 | 4.5 | 85.8 | 2.10 | 1.80 | 0.29 | 9.4 | 5.27 |
| (b) | 05-05-06/02 | 182.9 | -11 | -8 | 150 | 190 | 0.73 | 30.0 | 94.2 | 1.91 | 1.80 | 0.30 | 17.3 | 5.26 |
| | 05-15-06/03 | 53.3 | -13 | -3 | 277 | 30 | 0.84 | 4.5 | 85.8 | 2.10 | 1.80 | 0.29 | 9.4 | 5.27 |
| (c) | 05-05-06/06 | 182.9 | -19 | -16 | 150 | 110 | 0.94 | 24.8 | 89.2 | 2.04 | 1.82 | 0.49 | 10.1 | 5.29 |
| | 05-15-06/11 | 53.3 | -19 | -9 | 277 | 30 | 0.84 | 4.5 | 85.8 | 2.10 | 1.80 | 0.50 | 9.4 | 5.27 |
| (d) | 05-05-06/04 | 182.9 | -17 | -14 | 151 | 190 | 0.73 | 30.0 | 94.2 | 1.92 | 1.81 | 0.50 | 17.5 | 5.33 |
| | 05-15-06/02 | 53.3 | -13 | -3 | 278 | 30 | 0.36 | 10.5 | 86.0 | 2.10 | 1.81 | 0.50 | 9.5 | 5.29 |

**Figure 19**. Scaling from 183- to 53-cm-Chord using Constant-$We_L$ Method. $V_R$, 150 kt.

scaled ice shape, two tests should be considered. The first would scale the main ice shape by matching $We_L$, $\beta_0 A_c$ and $n_0$. With *LWC* chosen arbitrarily and *MVD* selected to gain as close a match of $\beta_0$ as possible, matching the above three parameters determines the scale velocity, time and temperature.

The second test, to scale icing limit, needs only to match $\beta_0$. For this experiment, neither $n_0$ nor $We_L$ are restricted. Thus, velocity can be calculated to satisfy $\beta_{0,S} = \beta_{0,R}$ with *MVD* chosen for convenience. For stagnation freezing fraction, $n_0$, no less than 0.3, *LWC* and temperature seem to have little effect on icing limit as shown in figure 16, so they can be chosen more or less arbitrarily. But lower $n_0$ may produce runback ice accretion that could complicate the process of identifying icing limits. Therefore, one should select a static temperature and *LWC* such that the total temperature will be below -2°C and $n_0$ will be no less than 0.3. Additional testing for $n_0$ less than 0.3 is needed to better assess whether this method still works, so it should be used with caution. The accretion time needs only be long enough to accrete sufficient ice to define the icing limit.

Test-Condition Scaling of Main Ice Shape When Model Size Unchanged

In reference 2, it was noted that the calibrated envelope of an icing facility could leave some combinations of MVD and *LWC* unobtainable. Furthermore, substitutions for temperature are sometimes necessary. By applying test-conditions scaling, alternatives for each of these test conditions can often be found that fall within the facility capabilities yet provide an ice shape that simulates that of the reference (desired) conditions. Test-condition scaling methods for *LWC*, temperature and *MVD* will be discussed here.

*LWC* Scaling (The Olsen Method)

Earlier in this paper, it was demonstrated with figure 15 that the Olsen method, as a special case of the recommended scaling method, can be used to scale *LWC* over at least a limited range for both Appendix C and SLD conditions. The method used in reference 2 will therefore be recommended for SLD. This procedure is given as follows:

1. $c_S = c_R$.
2. $V_S = V_R$.
3. $MVD_S = MVD_R$.
4. Choose a $LWC_S$.
5. Calculate the scale temperature $t_{st,S,}$ from $n_{0,S} = n_{0,R}$.
6. Calculate the scale total temperature, $t_{tot,S}$. If $t_{tot,S}$ is greater than -2°C, repeat steps 4, 5 and 6 with a larger $LWC_S$.
7. Calculate the scale accretion time from $A_{c,S} = A_{c,R}$, which that leads to $\tau_S = (LWC_R \times \tau_R)/LWC_S$.

Temperature Scaling (The Olsen Method)

To apply the Olsen method for temperature scaling, the procedure is given as follows:

1. $c_S = c_R$.
2. $V_S = V_R$.
3. $MVD_S = MVD_R$.
4. Choose a scale static temperature $t_{st,S}$ so that the scale total temperature $t_{tot,S}$ is below -2°C.
5. Calculate $LWC_{S,}$ from $n_{0,S} = n_{0,R}$.
6. Calculate the scale accretion time from $A_{c,S} = A_{c,R}$ that leads to $\tau_S = (LWC_R \times \tau_R)/LWC_S$.

The Olsen method is based on a fundamentally sound approach, but has been experimentally validated over only a limited range of test conditions. Additional testing is needed to further validate this approach, so it should be used with caution.

*MVD* Scaling (to scale ice shape, not icing limits)

Figures 10-12 have shown, with a few exceptions, that *MVD* over the range 30 to 190 μm had no apparent effect on the main ice shape for the conditions and models tested. These observations imply that if a test is needed with a value of *MVD* outside the tunnel capability, it should be possible to substitute a value within the tunnel-operating map to simulate the desired ice shape. This procedure is outlined as follows:

1. $c_S = c_R$.
2. $V_S = V_R$.
3. Choose a $MVD_S$ such that $\beta_{0,S}$ and $\beta_{0,R}$ are within 10%.
4. Choose a $LWC_S$.
5. Calculate the scale temperature $t_{st,S,}$ from $n_{0,S} = n_{0,R}$.
6. Calculate the scale total temperature, $t_{tot,S}$. If $t_{tot,S}$ is greater than -2°C, repeat steps 4, 5 and 6 with a larger $LWC_S$.
7. Calculate the scale accretion time $\tau_S$ from $\beta_{0,S} A_{c,S} = \beta_{0,R} A_{c,R}$.

There are some *MVD* limits (not known yet) to this approach, however. The observation that drop size has little effect on main ice shape as shown in figures 10-12 comes from only limited testing over a specific range of test conditions. Therefore, some caution may be warranted for application to other conditions. Tests over a wider range of speed, model size and cloud conditions are needed to better assess whether the robustness of a method of drop-size substitution can be recommended with any confidence. Tests of this nature are currently being conducted at the NASA Glenn IRT for both Appendix C and SLD conditions to try to define the upper and lower limits of conditions for which an available *MVD* can be used in an icing test to simulate results with another *MVD*.

## Summary and Concluding Remarks

This paper has summarized recent NASA research into scaling of SLD conditions. It was shown that for NACA 0012 models up to 183-cm chord, reference velocities of 100, 150 and 200 kt, reference *MVD*s up to 190 μm and scale *MVD*s of approximately 30 μm at the stagnation point freezing fractions of both 0.30 and 0.50, the main difference in SLD ice accretions compared with Appendix C is that in SLD larger feather features can sometimes form aft of the main ice shape, particularly for velocities of around 150 kt and higher and when $\beta_0$ is above 90%. Thus, these large feather structures appear to be the result of high collection efficiencies. Not only do SLD clouds have higher *MVD*s the drop-size distributions contain significantly larger water drops, and these likely contribute to large feather formations. When the scale $\beta_0$ matches the reference value, however, the evidence suggests that scale and reference feather sizes tend to be approximately the same.

Because the features of the main ice shape do not appear to be affected by drop size, it is safe to conclude that, for models as large as 183-cm chord, drop sizes from 30 to 190-μm *MVD* and velocities of 200 kt or less, SLD main ice shapes are not subject to significant differences in the effects of drop distortion and breakup before impact or splashing of drops on impact compared with those in Appendix C. This may mean that these effects are scaled appropriately between Appendix C and SLD conditions using the existing scaling methods. These conclusions may not apply to the feather regions, where accretion mechanisms are not yet understood. Fortunately, therefore, scaling methods that have been found to be effective for Appendix C can also be applied to at least the limited range of SLD conditions included in this study. The currently recommended methods to scale model size, icing limit and test conditions are outlined in the section Recommended Scaling Methods on p 27.

The main ice shape from a 183-cm-chord NACA 0012 model was successfully simulated with a 27-cm-chord model (fig. 18) using the scaling method described on p 27. Tests for this model-size scale ratio were limited to a reference velocity of 100 kt to avoid very high scale velocities. Using the same reference model, good model-size scaling was also demonstrated for a reference velocity of 150 kt when a scale model of 53-cm chord was used (fig. 19). Finally, scaling from a 91- to 36-cm chord was exhibited with a reference velocity of 200 kt (fig. 17).

It was shown in figure 16 that the icing limit is a function only of the stagnation collection efficiency, $\beta_0$ when $n_0$ is greater than 0.3. Therefore, tests to determine experimental icing limits with a scale model and a *MVD* chosen for convenience can be made simply by matching scale and reference $\beta_0$. Equations (2) – (6) provide expressions to calculate $\beta_0$. To avoid potential runback icing due to lower $n_0$, one selects a static temperature and *LWC* so that the total temperature will be below -2°C and $n_0$ will be no less than 0.3. Additional testing is needed to further validate this approach for $n_0$ less than 0.3, so it should be used with caution.

To scale *LWC*, it was shown that for SLD conditions as for Appendix C the Olsen method could be used (fig. 15). That method requires that with a full-size model and with scale *V* and *MVD* matched to the respective reference conditions one chooses a scale *LWC* and the scale temperature should be determined by matching the scale $n_0$ to the reference. Care may be needed to ensure that the scale total temperature is below-2°C. The scale accretion time is found by matching scale and reference $A_c$. The stagnation freezing fraction, $n_0$, can be found from equations (7) – (10), and $A_c$ from equation (1). Similarly, the Olsen method can also be used to scale temperature. It requires that with a full-size model and with scale *V* and *MVD* matched to the respective reference conditions one chooses a scale static temperature so that the scale total temperature is below -2°C.and the scale *LWC* should be determined by matching the scale $n_0$ to the reference. The scale accretion time is found by matching scale and reference $A_c$. The stagnation freezing fraction, $n_0$, can be found from equations (7) – (10), and $A_c$ from equation (1).

Furthermore, if a *MVD* scaling is needed for a test due to tunnel limitations, it was shown, at least for the range of speed, model size and cloud conditions tested in this study, that with model size and velocity unchanged from the reference, one can choose a *MVD* such that the scale and reference $\beta_0$ are within 10% and a *LWC* for

convenience. The scale temperature should be determined by matching the scale $n_0$ to the reference. Again, care may be needed to ensure that the scale total temperature is below-2°C. The scale accretion time is found by matching scale and reference $A_c$

The studies on which these recommendations are based were performed with numerous limitations. All used unswept NACA 0012 models (up to 183-cm chord) mounted at 0° angle of attack. The tests covered a range of reference velocities of 100, 150 and 200 kt, *MVD*s of approximately 25 to 190 μm and stagnation freezing fractions of both 0.30 and 0.50. Because no tests in the present study have been performed for *MVD*s greater than 190 μm, there is no basis to assume the scaling method described here would be valid to scale clouds with larger *MVD*s. Finally, the largest model used to date had a chord of 183 cm. SLD effects such as drop distortion and breakup on larger models may give different results.

Several issues need to be resolved in future SLD scaling studies. First, the upper limit on *MVD* for which SLD main ice shapes can be simulated by Appendix C drop sizes needs to be determined. This limit may also depend on model size and velocity. Likewise, the lower limit on scale *MVD* also needs to be determined. Rime tests by Tsao and Anderson[38] showed significantly narrower shapes with different profiles for drop sizes below about 20 μm. Thus, it is possible, although not confirmed, that glaze ice shapes for *MVD*s significantly smaller than 25 μm may prove to be poor simulations of larger sizes. On the other hand, figure 3.3.6 of reference 2 reproduced limited results for $n_0$ of 0.3 and 0.5 showing that *MVD*s of 20 and 55 μm produced the same ice shape, and, for other conditions, figure 3.3.7 of that reference showed that no difference in shape between 15 and 20 μm was apparent for $n_0$ of 0.5. More extensive studies of these small *MVD*s are needed. Until this is done, it is advised that if scale calculations based on matching $\beta_0$ yield scale *MVD*s of, say, 15 or 20 μm, caution should be used in interpreting the results of such scale tests. At least some additional tests should be performed at 25 – 30 μm for comparison. Second, the physical mechanism that produces the very large feather structures aft of the main ice shape for some SLD conditions has to be explored and comprehended. It appears that these feathers are produced because the local $\beta$ values for SLD encounters are often higher than those for Appendix C, but this explanation has not been fully tested. Third, the method used here for model-size scaling in glaze icing uses a match of $We_L$ to determine scale velocity. Although this approach seems to work, the physics behind it are not understood, nor do we know if there is a better Weber number or other similarity parameter to use. Without a full understanding, it is not safe to extrapolate the method to conditions not yet tested.

Finally, scaling needs to be demonstrated with models other than the NACA 0012, with angle of attack, with swept wings and in facilities other than the IRT. The use of a different test facility, provided it has a uniform cloud with a consistent calibration over the range of conditions of interest, should not affect scaling outcomes. Furthermore, the basic physics behind the development of the scaling method recommended here is independent of the model, of angle of attack and of sweep angle. Nevertheless, additional demonstrations of scaling in various configurations will serve to build confidence in the method.

## References


[1] Code of Federal Regulations, Title 14, Chapter I, Federal Aviation Administration, Department of Transportation, Part 25, "Airworthiness Standards: Transport Category Aircraft," Appendix C, U.S. Government Printing Office, Washington DC, revised as of January 2005.

[2] Anderson, David N., "Manual of Scaling Methods," NASA/CR—2004-212875, March 2004.

[3] Ruff, Gary A., "Analysis and Verification of the Icing Scaling Equations," AEDC-TR-85-30, vol 1 (rev), March 1986.

[4] Olsen, William and Newton, James, "Experimental and Analytical Evaluation of Existing Icing Scaling Laws," unpublished draft of NASA Technical Memorandum, 1986.

[5] Bartlett, C. Scott, "Icing Scaling Considerations for Aircraft Engine Testing," AIAA-88-0202, January 1988.

[6] Bartlett, C. Scott, "An Empirical Look at Tolerances in Setting Icing Test Conditions with Particular Application to Icing Similitude," DOT/FAA.CT-87/31 and AEDC-TR-87-23, August 1988.

[7] Oleskiw, Myron M., De Gregorio, Fabrizio and Esposito, Biagio, "The Effect of Altitude on Icing Tunnel Airfoil Icing Simulation," *Proceedings of the FAA International Conference on Aircraft Inflight Icing*, DOT/FAA/AR-96/81,II, August 1996, pp511-520.

[8] De Gregorio, F. and Esposito, B., "Prove Sperimentali sull'Accrescimento del Ghiaccio al Variare della Quo-

ta," CIRA Report MC-3E-CIRA-5-TR-0023, February 1996.

[9] De Gregorio, F. and Imperato, L., "Experimental Assessment of Icing Scaling Laws," CIRA Document MC-3E-CIRA-7-TR-0033, August 1996.

[10] Esposito, Biagio M., Ragni, Antonio, Ferrigno, Francesco and Vecchione, Ludovico, "Cloud Calibration Update of the CIRA Icing Wind Tunnel," SAE 2003-01-2132, June 2003.

[11] Ragni, A., Esposito, B., Marrazzo, M., Bellucci, M. and Vecchione, L., "Calibration of the CIRA IWT in the High Speed Configuration," AIAA-2005-471, January 2005.

[12] Langmuir, Irving and Blodgett, Katharine B.: "A Mathematical Investigation of Water Droplet Trajectories," Army Air Forces Technical Report No. 5418, February 1946.

[13] Abbott, Ira H. and von Doenhoff, Albert E., *Theory of Wing Sections*, Dover, New York, 1959, pp114 and 321.

[14] Wright, William B., "Further Refinements of the LEWICE SLD Model," AIAA-2006-464, January 2006.

[15] Wright, William B., unpublished LEWICE 3.2 validation ice-shape predictions.

[16] Messinger, B.L., "Equilibrium Temperture of an Unheated Icing Surface as a Function of Airspeed," *J. Aeron. Sci.*, vol. 20 no. 1, January 1953, pp 29 – 42.

[17] Tribus, Myron, Young, G.B.W. and Boelter, L.M.K., "Analysis of Heat Transfer Over a Small Cylinder in Icing Conditions on Mount Washington," *Trans. ASME*, vol. 70, November 1948, pp 971 – 976.

[18] Charpin, Francois and Fasso, Guy, "Essais de givrage dans la grande soufflerie de Modane sur maquettes a echelle grandeur et echelle reduite," *L'Aeronautique et l'Astronautique*, no. 38, 1972, pp 23 – 31. English translation published as "Icing Testing in the Large Modane Wind-Tunnel on Full-Scale and Reduced Scale Models," NASA TM-75373, March 1979.

[19] Bilanin, Alan J., "Proposed Modifications to Ice Accretion/Icing Scaling Theory," *J. Aircraft*, vol 28, no 6, June 1991, pp 353-359.

[20] Bilanin, Alan J. and Anderson, David N., "Ice Accretion with Varying Surface Tension," AIAA-95-0538 and NASA TM 106826, January 1995.

[21] Soeder, Ronald H., Sheldon, David W., Ide, Robert F., Spera, David A. and Andracchio, Charles R., "NASA Glenn Icing Research Tunnel User Manual," NASA/TM–2003-212004, September 2003.

[22] Oldenburg, John R., Ide, Robert F., Del Roso, Richard L. and Murphy, Patrick J., "Improvements to the NASA Glenn Icing Research Tunnel's Air Temperature Measurement System," AIAA-2006-1222, January 2006.

[23] Tsao, Jen-Ching and Anderson, David N., "Further assessment of MVD Effects in SLD Applications," AIAA-2005-0072, January 2005 and NASA/CR—2006-214125, February 2006.

[24] Tsao, Jen-Ching and Anderson, David N., "Latest Developments in SLD Scaling," AIAA-2005-5187, June 2005 and NASA/CR—2006-214127, February 2006.

[25] Ide, Robert F., unpublished 2006 IRT SLD calibration.

[26] SigmaScan Pro version 5, Systat Software, Inc.

[27] Luxford, Geoffrey, Hammond, David W. and Ivey, Paul, "Role of Droplet Distortion and Break-up in Large Droplet Aircraft Icing," AIAA-2004-411, January 2004.

[28] Wright, William B. and Potapczuk, Mark G., "Semi-Empirical Modeling of SLD Physics," AIAA-2004-0412, January 2004 and NASA/TM—2004-212916, April 2004.

[29] Wright, William B., "Computational Simulation of Large Droplet Icing," *Proceedings of the FAA International Conference on Aircraft Inflight Icing* vol. II, DOT/FAA/AR-96/81,II, August 1996, pp 545 – 555.

[30] Mundo, C., Sommerfeld, M. and Tropea, C., "Droplet-Wall Collisions: Experimental Studies of the Deformation and Breakup Process," Int. J. Multiphase Flow, vol 21, no. 2, 1995, pp151 – 173.

[31] Potapczuk, Mark G., "Ice Mass Measurements: Implications for the Ice Accretion Process," AIAA-2003-387, January 2003.

[32] Papadakis, Michael, Rachman, Arief, Wong, See-Cheuk, Bidwell, Colin and Bencic, Timothy, "An Experimental Investigation of SLD Impingement on Airfoils and Simulated Ice Shapes," SAE 2003-01-2129.

[33] Rutkowski, Adam, Wright, William B. and Potapczuk, Mark, "Numerical Study of Droplet Splashing and Re-impingement," AIAA-2003-388, January 2003.

[34] Tan, S.C. and Papadakis, M., "General Effects of Large Droplet Dynamics on Ice Accretion Modeling," AIAA-2003-392, January 2003.

[35] Gent, Roger W., Ford, James M., Moser, Richard J. and Miller, Dean R., "Results from SLD Mass Loss Tests in the ACT Luton Icing Wind Tunnel," AIAA-2003-0389, January 2003.

[36] Gent, R.W., Ford, J.M., Moser, R.J. and Miller, D.R., "SLD Research in the UK," SAE 2003-01-2128, June 2003.

[37] Anderson, David N. and Tsao, Jen-Ching, "Additional Results of Ice-Accretion Scaling at SLD Conditions," AIAA-2003-0390, January 2003 and NASA/CR—2005-213850, August 2005.

[38] Tsao, Jen-Ching and Anderson, David N., "Additional Study of MVD Effects on Ice Shapes," AIAA-2004-0413, January 2004 and NASA/CR—2005-213853, August 2005.

| REPORT DOCUMENTATION PAGE | Form Approved OMB No. 0704-0188 |
|---|---|



| 1. REPORT DATE *(DD-MM-YYYY)* | 2. REPORT TYPE | 3. DATES COVERED *(From - To)* |
|---|---|---|
| 01-09-2008 | Final Contractor Report | |

**4. TITLE AND SUBTITLE**
Ice Shape Scaling for Aircraft in SLD Conditions

**5a. CONTRACT NUMBER**

**5b. GRANT NUMBER**

**5c. PROGRAM ELEMENT NUMBER**
NNC07BA13B

**6. AUTHOR(S)**
Anderson, David, N.; Tsao, Jen-Ching

**5d. PROJECT NUMBER**

**5e. TASK NUMBER**

**5f. WORK UNIT NUMBER**
WBS 457280.02.07.03.02

**7. PERFORMING ORGANIZATION NAME(S) AND ADDRESS(ES)**
National Aeronautics and Space Administration
John H. Glenn Research Center at Lewis Field
Cleveland, Ohio 44135-3191

**8. PERFORMING ORGANIZATION REPORT NUMBER**
E-16571

**9. SPONSORING/MONITORING AGENCY NAME(S) AND ADDRESS(ES)**
National Aeronautics and Space Administration
Washington, DC 20546-0001

**10. SPONSORING/MONITORS ACRONYM(S)**
NASA

**11. SPONSORING/MONITORING REPORT NUMBER**
NASA/CR-2008-215302

**12. DISTRIBUTION/AVAILABILITY STATEMENT**
Unclassified-Unlimited
Subject Category: 03
Available electronically at http://gltrs.grc.nasa.gov
This publication is available from the NASA Center for AeroSpace Information, 301-621-0390

**13. SUPPLEMENTARY NOTES**

**14. ABSTRACT**
This paper has summarized recent NASA research into scaling of SLD conditions with data from both SLD and Appendix C tests. Scaling results obtained by applying existing scaling methods for size and test-condition scaling will be reviewed. Large feather growth issues, including scaling approaches, will be discussed briefly. The material included applies only to unprotected, unswept geometries. Within the limits of the conditions tested to date, the results show that the similarity parameters needed for Appendix C scaling also can be used for SLD scaling, and no additional parameters are required. These results were based on visual comparisons of reference and scale ice shapes. Nearly all of the experimental results presented have been obtained in sea-level tunnels. The currently recommended methods to scale model size, icing limit and test conditions are described.

**15. SUBJECT TERMS**
Icing scaling; Icing physics

| 16. SECURITY CLASSIFICATION OF: | | | 17. LIMITATION OF ABSTRACT | 18. NUMBER OF PAGES | 19a. NAME OF RESPONSIBLE PERSON |
|---|---|---|---|---|---|
| a. REPORT | b. ABSTRACT | c. THIS PAGE | | | STI Help Desk (email:help@sti.nasa.gov) |
| U | U | U | UU | 41 | 19b. TELEPHONE NUMBER *(include area code)* 301-621-0390 |